NUMERICAL MEASURE OF SPLITTING ANGLE

J. FÉJOZ, V. KALOSHIN, M. GUARDIA, P. ROLDÁN

ABSTRACT. Goal: measure splitting of stable/unstable manifolds of a resonant periodic orbit in the Sun-Jupiter RTBP.

1. Periodic Orbit

1.1. **2-body problem.** Vadim has provided us an initial condition that corresponds to a 7:1 resonant periodic orbit in Kepler's problem (polar coordinates)

$$H = \frac{1}{2}(R^2 + \frac{\Theta^2}{r^2}) - \frac{1}{r}.$$

The initial condition is at the perihelion,

$$(r, R, \theta, \Theta) = (1.302533194, 0.0, 0.0, 1.46336205),$$

or equivalently in euclidean coordinates

$$(x, y, v_x, v_y) = (1.302533194, 0.0, 0.0, 1.123473908).$$

This periodic orbit lives in the energy level $H = -1.6$.

In fact, we have a program that, given an energy value H, computes an initial condition of Asteroid (x, y, v_x, v_y) corresponding to $r = p/q$ ressonant periodic orbit in the 2BP. Here, p is period of asteroid and q is period of Jupiter. We impose that initial condition is at the perihelion. This implies that position of Asteroid is $A = (x, 0)$ and velocity is $v = (0, v_y)$. Therefore, we output as initial condition only the components (x, v_y).

```
roldan@pollo:~/research/splitting/initcond$ initcond
-1.6 7                                          # input: H r=p/q
1.302533194285694e+00 1.123473908222282e+00   # output: x v_y
```

First of all, we check that this initial condition is correct. An analytical integration of Kepler's equations gives the particular solution

$$u = 1/r, \quad u(\theta) = 1/c^2(1 + \epsilon\cos(\theta - g)),$$

with constant angular momentum $c = 1.46336205$, eccentricity $\epsilon = 0.644049091$, and argument of the perihelium $g = 0$. Since $0 < \epsilon < 1$, it is an ellipse.

Moreover, we have integrated the trajectory numerically, and indeed we obtain a periodic orbit of period $T = 14\pi$ with high precision. Program "ikepler" integrates the trajectory:

```
roldan@pollo:~/research/splitting/ikepler$ ./ikepler <ikepler.dat
0.000000e+00 1.302533e+00 0.000000e+00 0.000000e+00 1.463362e+00
...
4.398230e+01 1.302533e+00 -2.501898e-08 6.283185e+00 1.463362e+00
```

The first line corresponds to the initial condition $(t = 0, r, R, \theta, \Theta)$ and the last line to the final point $(t = 14\pi, r, R, \theta, \Theta)$. Note that they only differ by 10^{-8} (the first column is just time, and the fourth column is an angle, so $6.283185e + 00 = 0 \pmod{2\pi}$.

See a plot of the trajectory in figure 1.

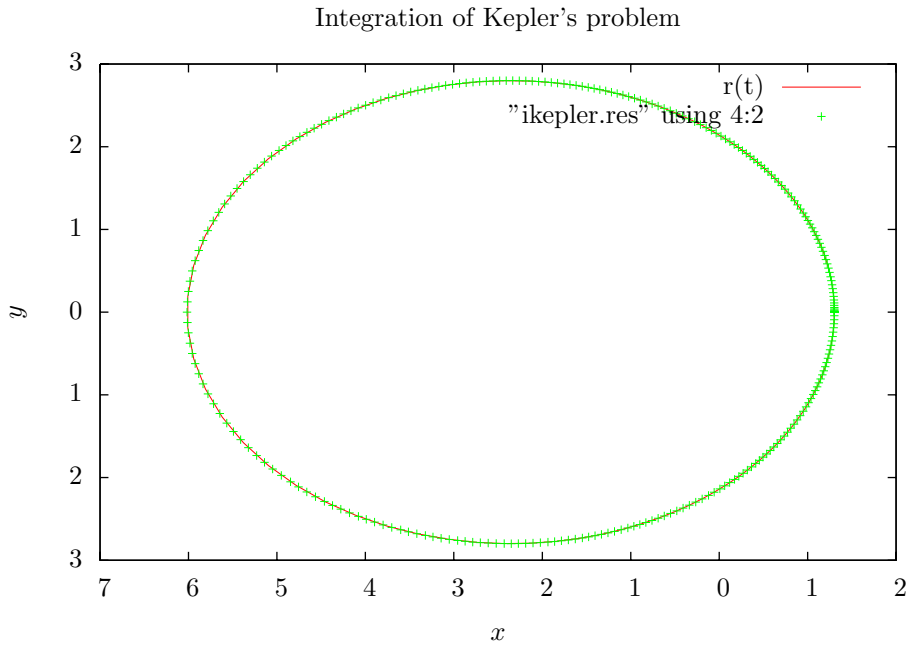

FIGURE 1. Integration of Kepler's problem: analytical trajectory in red, numerical in green.

1.2. **3-body problem.** Now we switch to the (circular, planar) RTBP equations (in synodical, or rotating, coordinates)

$$H(x,y,p_x,p_y) = \frac{1}{2}(p_x^2+p_y^2) + yp_x - xp_y - \frac{\mu_1}{r_1} - \frac{\mu_2}{r_2}, \tag{1}$$

where

$$r_1^2 = (x-\mu_2)^2 + y^2,$$
$$r_2^2 = (x+\mu_1)^2 + y^2.$$

We follow the convention to place the large mass (Sun) to the left of the origin, and the small mass (Jupiter) to the right. (This is opposite to the astrodynamics convention). Thus we choose $\mu_1 = \mu$ as the small mass, and $\mu_2 = 1-\mu$ as the large mass.

We would like to check that the initial condition for the 2BP is still a good approximation to a resonant periodic orbit in the RTBP.

As a first test, we consider the RTBP (1) with $\mu = 0$. This is just the 2BP in rotating coordinates (position-momentum instead of position-velocity). We need to express the initial condition in these RTBP coordinates. Note that the origin is still located at the Sun. Since the initial condition is at the perihelion, at $t = 0$ the rotating and fixed frame coincide, so $(x,y)_{\text{2BP}} = (x,y)_{\text{RTBP}}$.

Moreover, remember the interpretation of momenta in the rotating system: p_x, p_y are the components of the velocity (wrt the fixed system) along the rotating axes (see Szebehelly, page 349). Again, since the rotating and fixed frame coincide, $(v_x,v_y)_{\text{2BP}} = (p_x,p_y)_{\text{RTBP}}$. Thus, it turns out that

$$(x,y,p_x,p_y)_{\text{RTBP}} = (x,y,v_x,v_y)_{\text{2BP}} = (1.302533194, 0.0, 0.0, 1.123473908).$$

Again, we compare the initial and final points after integrating time 14π. Program "frtbp" computes the flow of the RTBP.

Remark 1.1. We use a variable-order taylor method specially generated to integrate the equations of motion of the RTBP. The taylor method has been generated using the "taylor" package of À. Jorba and M. Zou (see `http://www.maia.ub.es/~angel/taylor/`). The main advantage of using a taylor method is that it is very fast for long-time integrations (without sacrificing accuracy).

```
roldan@pollo:~/research/splitting/frtbp$ frtbp
0                                                    # input: mu
43.98229715025710533816                              # input: 14\pi
1.302533194285694e+00 0.0 0.0 1.123473908222282e+00

# output:
1.302533194285696e+00 -3.183137881087434e-13         # x, y
1.708491712633289e-13 1.123473908222281e+00          # p_x, p_y
```

We input mass parameter $\mu = 0$ (first line), integration time $t = 14\pi$ (second line), and initial condition (third line). The program outputs the final point (fourth line). Notice that the distance between initial and final point is about 10^{-13}. Therefore we obtain a resonant periodic orbit.

As a second test, we consider the RTBP (1) with $\mu = 0.95387536e-3$, the mass ratio of Sun-Jupiter. Of course, the Sun is not located at the origin anymore, but nevertheless we hope that the same initial condition

$$(x, y, p_x, p_y)_{\text{RTBP}} = (1.302533194, 0.0, 0.0, 1.123473908)$$

gives rise to a trajectory that is close to a resonant periodic orbit. Let's check it again by applying the flow time 14π:

```
roldan@pollo:~/research/splitting/frtbp$ frtbp
0.95387536e-3
43.98229715025710533816
1.302533194285694e+00 0.0 0.0 1.123473908222282e+00

# output:
1.250163242561269e+00 -4.990618523763478e-01
2.444851824792766e-01 1.076199186094388e+00
```

and we see that the final and initial points (third and fourth lines) differ by about 10^{-1}. Therefore we are close to a resonant periodic orbit of the RTBP.

Next we refine the approximate periodic orbit into a "true" periodic orbit (up to numerical integration errors). Consider the Poincare section

$$\Sigma = \{y = 0,\ p_y > 0\}$$

in the autonomous RTBP (1), and let $P\colon\ \Sigma \to \Sigma$ be the associated Poincare map.

Notice that, in the rotating frame, a 7:1 resonant periodic orbit makes 6 turns around the origin. We look for the periodic orbit as a fixed point of the map

$$\mathcal{P} \equiv P^6,$$

which is the 6-th iterate of the Poincare map. We will refer to $\mathcal{P}$ as the *iterated Poincare map*.

Remark 1.2. Due to some symmetry of the RTBP equations w.r.t. the horizontal axis, in fact it is only necessary to integrate for half a period of the periodic orbit. We will exploit this fact in section 1.3.

For instance, let us compute the image $p' = \mathcal{P}(p) = P^6(p)$ of the point $p = (x, y, p_x, p_y) = (1.302533194, 0.0, 0.0, 1.123473908)$, which corresponds to our guess to the periodic orbit. Of course, we expect this to be close to a fixed point.

Remark 1.3. Numerical remark: A point is assumed to be on the Poincare section if it is within distance 10^{-16} to the section.

```
roldan@pollo:~/research/splitting/prtbp$ ./prtbp
0.95387536e-3                              #input: mu
6                                          #input: number of iterates
#input: (x,y,p_x,p_y)
1.302533194285694e+00 0.0 0.0 1.123473908222282e+00
#output:
1.693695656893852e+00                      # x'
4.879248589363672e-16                      # y'
-4.007796441169778e-01                     # p_x'
8.653917332089469e-01                      # p_y'
4.285874020770370e+01                      # integration time
```

Thus the Poincare iterate is very close to the input point. Moreover, as a side product, we also compute the integration time needed to reach the Poincare section. This number is of course close to $14\pi = 43.982\ldots$.

To further reduce dimensionality, fix the level of energy to

$$H(x, y, p_x, p_y) = H_0 = -1.6 \tag{2}$$

We look for the periodic orbit *in the energy manifold* H_0.

*** Does there exist a periodic orbit for every value of the energy close to H_o??? I guess so. ***

*** If there exists one, is it exactly resonant (i.e. does it have the *exact* period 14π)??? I guess not. Maybe we can look for the exact resonant periodic orbit by varying the energy level. ***

Using this energy condition (2), we can work with only two variables, (x, p_x). The variable $y = 0$ since we look at the Poincare section. Further, suppose $\partial H/\partial p_y \neq 0$ so we can apply IFT, and the variable p_y can be obtained from the energy condition (2). Given x, p_x, y and H, we just need to solve a quadratic equation for p_y.

```
roldan@pollo:~/research/splitting/hinv$ ./hinv
0.95387536e-3 -1.6                                    #input: mu, H
1.302533194285694e+00 0.0 0.0 1.123473908222282e+00   #input: p
hinv: I have chosen branch number 2
1.113427091316086e+00                                 #output: p_y
```

For instance, let us compute the 2-dimensional Poincare map $\mathcal{P}(p)$ of the point $p = (x, p_x) = (1.302533194, 0.0)$, which corresponds to our guess to the periodic orbit. Of course, we expect this to be close to a fixed point.

```
roldan@pollo:~/research/splitting/prtbp$ ./prtbp_2d
0.95387536e-3                              #input: mu
-1.6                                       #input: H
6                                          #input: number of iterates of P
1.302533194285694e+00 0.0                  #input: (x,p_x)
1.123473908222282e+00                      #input: p_y estimate

#output: (x',p_x') integration_time
hinv: I have chosen branch number 2
3.664378990446215e+00 3.061299749188896e-01 4.633168561934585e+01
```

Notice that we do not obtain the same point as with the 4D Poincare map. This is due to the fact that we are using an energy level $H = -1.6$ which, *for the RTBP*, does not correspond to the point $(x, y, p_x, p_y) = (1.3025, 0, 0, 1.1234)$. This was true only in the 2BP.

The corresponding energy level for the RTBP is

$$H(x, y, p_x, p_y) = -1.60184944512740670488.$$

Let us now use this energy level.

```
roldan@pollo:~/research/splitting/prtbp$ ./prtbp_2d
0.95387536e-3
-1.60184944512740670488
6
1.302533194285694e+00 0.0
1.123473908222282e+00

#output: (x',p_x') integration_time
hinv: I have chosen branch number 2
1.693695656894214e+00 -4.007796441170626e-01 4.285874020770324e+01
```

Of course, now we obtain the same point as with the 4D Poincare map.

Next we compute the derivative of the Poincare map. For each $\xi \in R^4$, let $u(t, \xi)$ be the solution of the system with initial condition $u(0, \xi) = \xi$. Let Σ be the Poincare section $\{y = 0\}$, and $T : \Sigma \to R$ the Poincare return time. The derivative of the Poincare map at a point p is given by the partial derivative $u_\xi(T(p), p)$. It is easy to see that $u_\xi(t, p)$ is the matrix solution of the variational equation

$$\dot{W} = Df(u(t, p))W,$$

where f is the vectorfield of the RTBP. We compute $u_\xi(T(p), p)$ by numerically integrating the variational equations.

```
roldan@pollo:~/research/splitting/dprtbp$ ./dprtbp
0.95387536e-3                           #input: mu
6                                       #input: number of iterates
#input: p=(x, y, p_x, p_y)
1.302533194285694e+00 0.0 0.0 1.123473908222282e+00

#output: u_\xi(T(p),p)
 1.163429283356999e+02 -5.605786501223135e+00 -2.674694568710321e+00  2.199226681825827e+02
-2.477782902512909e+02  1.000758275840821e+01  1.835082184567418e+00 -4.727484205470752e+02
 9.942019451626798e+01 -3.778309795557094e+00 -3.066006635286664e-01  1.891231152838540e+02
 5.840932484939698e-03  4.749823112392679e-01  9.251703062627508e-01  5.696378415895288e-01
```

Next we compute the derivative of the 2D Poincare map. Let $H(x, y, p_x, p_y)$ be the Hamiltonian of the RTBP (1). Let $f = (f_1, ..., f_4)$ be the vectorfield of the RTBP. Let $u(t, \xi) = \phi_t(\xi)$ be the flow of the RTBP. Let

$$u_\xi(T(p), p) = (u_{ij})_{i,j=1,...,4}$$

be the variationals, i.e. the derivative of the 4D Poincare map.

We want to compute

$$DP(x, p_x) = \begin{pmatrix} D_{11} & D_{12} \\ D_{21} & D_{22} \end{pmatrix}.$$

Let us compute D_{11} for example. Consider the first component of the 2D Poincare map, $P_1(x, p_x) = u_1(T(p), p) = u_1(T, x, 0, p_x, p_y(x, p_x))$. Take the partial derivative

$$D_{11} = \frac{\partial P_1}{\partial x} = \frac{\partial u_1}{\partial x} + \frac{\partial u_1}{\partial p_y}\frac{\partial p_y}{\partial x} + \frac{\partial u_1}{\partial T}\frac{\partial T}{\partial x}.$$

The following data is known:

$$\frac{\partial u_1}{\partial x} = u_{11}, \quad \frac{\partial u_1}{\partial p_y} = u_{14}, \quad \frac{\partial u_1}{\partial T} = f_1(u(T,p)).$$

It remains to find $\frac{\partial p_y}{\partial x}, \frac{\partial T}{\partial x}$. Consider the energy condition

$$H(x, 0, p_x, p_y(x, p_x)) = h.$$

Derivating wrt x, we obtain:

$$\frac{\partial p_y}{\partial x} = -\frac{\partial H/\partial x}{\partial H/\partial p_y} = \frac{f_3(p)}{f_2(p)}.$$

Consider the Poincare section condition

$$u_2(T, x, 0, p_x, p_y(x, p_x)) = 0.$$

Derivating wrt x, we obtain:

$$\frac{\partial T}{\partial x} = -\frac{1}{f_2(u(T,p))}\left(u_{21} + u_{24}\frac{\partial p_y}{\partial x}\right).$$

Therefore

$$D_{11} = u_{11} + u_{14}\frac{f_3}{f_2} + f_1(u(T,p))\left(-\frac{1}{f_2(u(T,p))}\left(u_{21} + u_{24}\frac{f_3}{f_2}\right)\right).$$

Similarly, we have

$$D_{12} = u_{13} - u_{14}\frac{f_1}{f_2} + f_1(u(T,p))\left(-\frac{1}{f_2(u(T,p))}\left(u_{23} - u_{24}\frac{f_1}{f_2}\right)\right),$$

$$D_{21} = u_{31} + u_{34}\frac{f_3}{f_2} + f_3(u(T,p))\left(-\frac{1}{f_2(u(T,p))}\left(u_{21} + u_{24}\frac{f_3}{f_2}\right)\right),$$

$$D_{22} = u_{33} - u_{34}\frac{f_1}{f_2} + f_3(u(T,p))\left(-\frac{1}{f_2(u(T,p))}\left(u_{23} - u_{24}\frac{f_1}{f_2}\right)\right).$$

Note that, in order to compute the 2D derivative $DP(x, p_x)$, it is enough to know the vectorfield f evaluated at the point p and at the point $u(T, p)$, and the variationals u_ξ evaluated at the point p.

```
roldan@pollo:~/research/splitting/dprtbp$ ./dprtbp_2d
0.95387536e-3 -1.6
6
1.302533194285694e+00 0.0
1.123473908222282e+00

#output: DP(x,p_x)
 3.2531386943e+02  1.3015817661e+00
-3.8740489754e+01 -1.5190784893e-01
```

To test the 2D derivative, we compute the *numerical* derivative of the 2D Poincare map at the point p using a central difference algorithm with one step of extrapolation. Then we compare the analytical and the numerical derivative.

```
roldan@pollo:~/research/splitting/dprtbp$ ./dprtbp_2d_test
0.95387536e-3                          #input: mu
-1.6                                   #input: H
6                                      #input: number of iterates
1.302533194285694e+00 0.0              #input: (x,p_x)

#output: test DP^n(x)
Estimate of absolute error in numerical derivative:
 2.1254818732e-05  1.7843979086e-06
```

```
 2.4934035771e-06  2.2582187636e-07
Discrepancy between analytical and numerical derivative:
-8.7975191718e-06 -5.9428008565e-06
 9.9582303648e-07  3.2423553453e-07

#output: test DP^{-n}(y)
Estimate of absolute error in numerical derivative:
 7.3360037329e-07  2.7119756323e-07
 4.2676801798e-05  8.4918256872e-05
Discrepancy between analytical and numerical derivative:
 4.7597529798e-07  2.9834163917e-07
 4.2294506144e-05 -1.0114603657e-04

#output: DP^n(x) DP^{-n}(y) = Id
 1.000000002977532e+00  2.500258031168379e-08
-3.528116418807792e-10  9.999999970374032e-01
```

It can be observed that the discrepancy between the analytical and numerical derivative is of the order of the estimated error commited in computing the numerical derivative.

In order to find a periodic orbit, we look for a fixed point of $p' = \mathcal{P}(p)$. To refine the (approximate) fixed point, we use a Newton-like method.

Remark 1.4. Numerical remark. Specifically, the Newton-like method we use is a modified version of Powell's Hybrid method (see the GSL manual for details) without scaling. We have tried other numerical methods (Newton's method, Hybrid method with internal scaling, etc) but they didn't work as well (failed to converge for some energy values).

We ask for an accuracy of 10^{-14} in finding the fixed point, i.e. a point $p = (x, p_x)$ is accepted as a fixed point iff the distance between the point and its poincare iterate is $dist(p, p') < 10^{-14}$.

1.3. **Symmetric periodic orbits.** We will use an alternative method to find periodic orbits. Since we are looking for *symmetrical* periodic orbits (with respect to the horizontal axis), it is enough to impose the condition that the trajectory after half the period is on the horizontal axis and has velocity $\dot{x} = 0$ (with 10^{-14} accuracy).

```
# Symmetric resonant 7:1 periodic orbit:
roldan@pollo:~/research/splitting/portbp$ ./portbpsym
0.95387536e-3 -1.6                    #input: mu, H
3                                     #input: iterates
1.302533194285694e+00                 #input: x (guess from 2BP)

# Newton iteration starts...
iter =   1 x =  1.2985595007, PX =  3.0329e-04
iter =   2 x =  1.2985841142, PX =  2.3411e-08
iter =   3 x =  1.2985841161, PX =  2.8460e-15
# output: x, period/2
1.298584116092567e+00 2.200898449498355e+01
```

Thus we find a symmetric periodic orbit $\Gamma_{7:1}$ passing through the point

$$p^* = (x, p_x) = (1.298\ldots, 0),$$

with almost-resonant period

$$T_{7:1} = 44.017\cdots \simeq 14\pi.$$

As a test, notice that the result for $\Gamma_{7:1}$ computed by this new method (exploiting the symmetry) is iqual to the one computed by the method of section 1 (not exploiting symmetry).

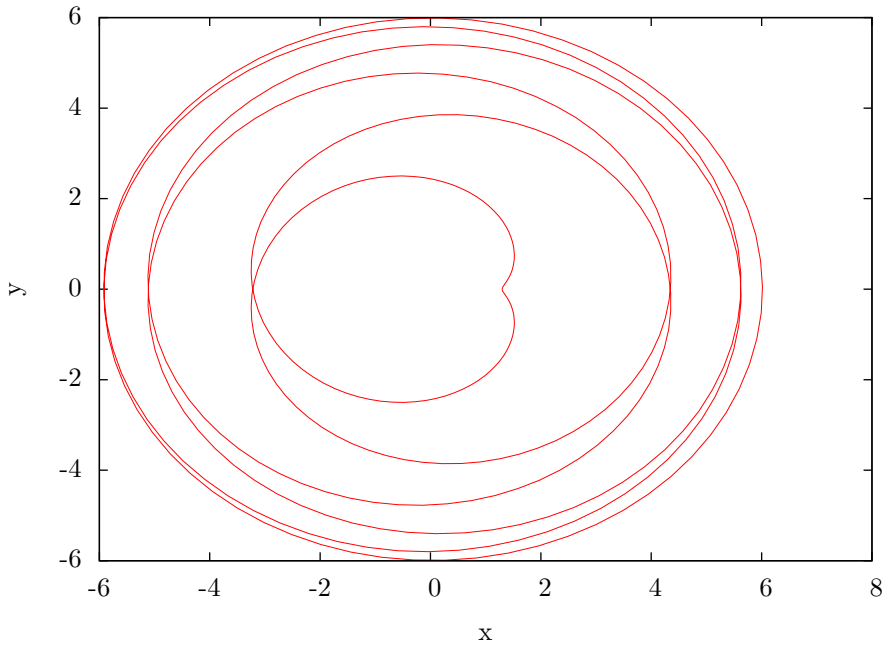

FIGURE 2. Periodic orbit of RTBP in rotating coordinates.

We plot the periodic orbit of the RTBP in figure 2. Figure 2 shows that, in rotating coordinates, the trajectory of the Asteroid makes 6 turns around the origin before closing up at the point p^*.

Figure 3 shows the same RTBP trajectory, but in fixed coordinates. It is worth mentioning that, in fixed coordinates, this orbit does *not* close up after time $T_{7:1}$. (In the picture it looks like it does, but actually it does not). This is due to the fact that the frequency associated to g in Delaunay variables is not necessarily resonant with the frequency associated to time. In any case, this trajectory is very close to the Kepler trajectory found before.

2. Resonant family of periodic orbits

Finally, we have also investigated other energy levels for the existence of a periodic orbit, and the dependence of the period $T(H)$ with respect to the energy level H. We obtain the results shown in figure 4.

Let $H_- = -2.04$ and $H_+ = -1.57$. For all energy levels $H \in [H_-, H_+]$, the Newton method converges and we are able to find a periodic orbit with high accuracy.

As seen in figure 4, period $T(H)$ increases with energy H. Notice that period tends to $14\pi = 43.982\ldots$ as energy tends to the endpoint H_-.

Let us plot the extremal periodic orbits of the family, i.e. the orbits that correspond to the endpoints H_- and H_+. See figure 5. The extremal periodic orbit with $H = H_-$ is very circular, and it passes far from Sun and Jupiter. The extremal periodic orbit with $H = H_+$ is very elliptical, and it passes very close to Jupiter (Jupiter orbits the circle of radius 1). In fact, the Newton method probably fails to

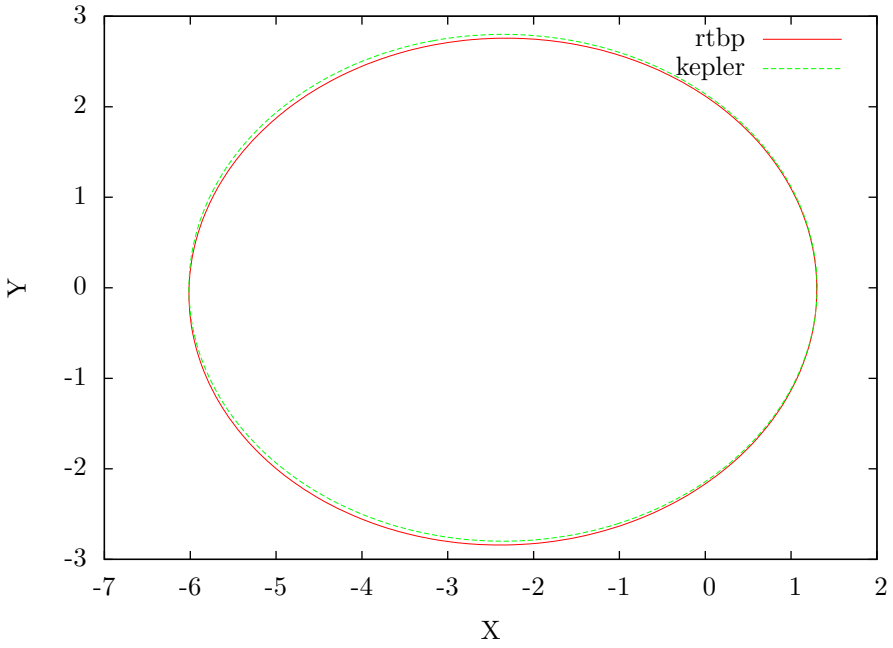

FIGURE 3. "Periodic" orbit in fixed coordinates (in red). For comparison, we replot Kepler's trajectory obtained in figure 1 (in green).

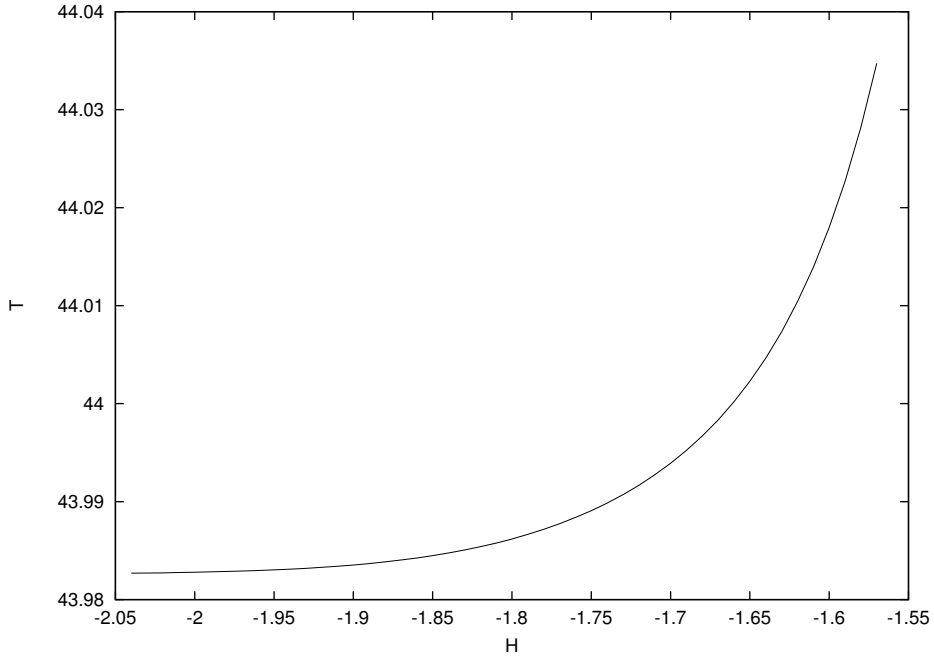

FIGURE 4. Resonant family of periodic orbits. We show period T as a function of energy level H.

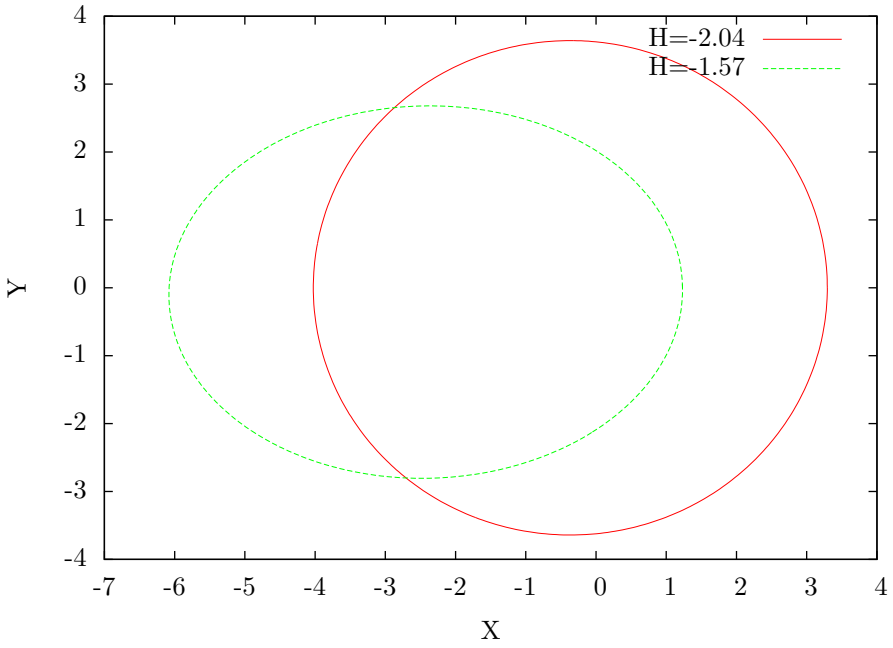

FIGURE 5. Extremal periodic orbits of the family: circular periodic orbit with $H = H_-$ (in red), elliptical periodic orbit with $H = H_+$ (in green).

converge past H_+ due to the fact that the periodic orbits tend to the asymptotic manifolds $W^{u/s}(L_2)$ of the collinear equilibrium point L_2.

We want to verify that the family of periodic orbits is close to the resonance, i.e. that the L component stays close to the value $7^{1/3}$. Let γ_H be the periodic orbit with energy level H. Integrating the periodic orbit in Delaunay coordinates $\gamma_H(t) = (l(t), L(t), g(t), G(t))$ over one period T_H, we compute the quantity

$$L_{\max}(H) = \max_{t\in[0,T_H)} |L(t) - 7^{1/3}|. \tag{3}$$

The function $L_{\max}(H)$ is plotted in figure 6. Notice that we obtain $|L(t)-7^{1/3}| < 7\mu$ for all $t \in \mathbb{R}$.

3. Hyperbolic Splitting

In this section, we compute the hyperbolic splitting associated to the resonant family of periodic orbits, i.e. to the NHIM.

First we consider the periodic orbit Γ with $H = -1.6$ that we found in section 1. Specifically, we will work with the periodic orbit corresponding to the fixed point

$$p^* = (x, p_x) = (1.298\ldots, 0),$$

of the iterated Poincare map $\mathcal{P}$.

Next we compute the derivative of $\mathcal{P}$ evaluated at p^*.

```
roldan@pollo:~/research/splitting/dprtbp$ dprtbp_2d
0.95387536e-3                          #input: mu
-1.6                                   #input: H
6                                      #input: number of iterates
1.298584116092567e+00 0                #input: p^*
```

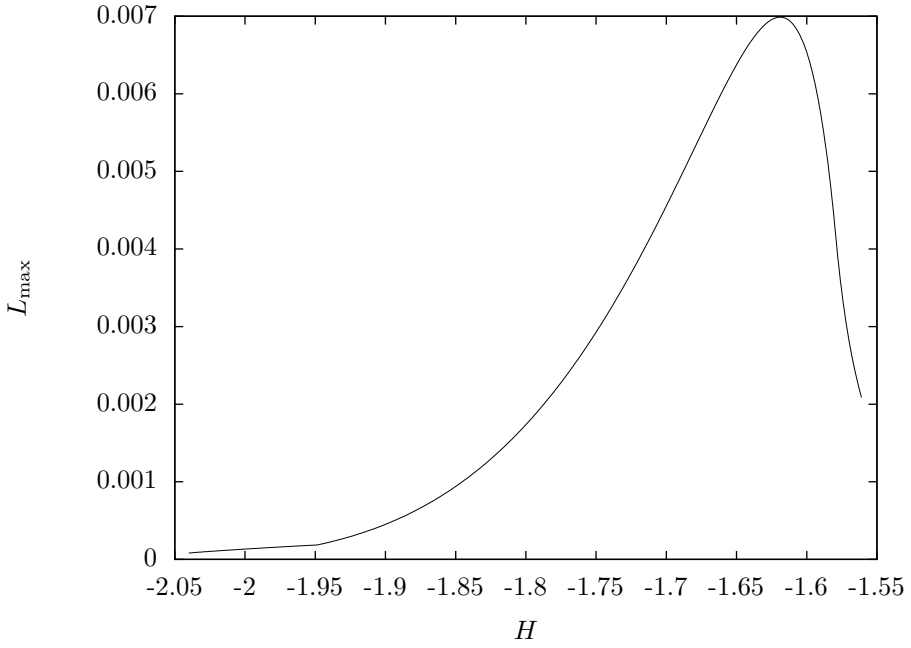

FIGURE 6. Maximum deviation of the square of semi-major axis L with respect to the resonant value $7^{1/3}$, see equation (3).

```
#output: DP(x,p_x)
 1.1828184291e+01  3.7987648894e-02
 3.6566080689e+03  1.1828184278e+01
```

We compute the characteristic multipliers of the variational equation along Γ, i.e. the eigenvalues ρ_u, ρ_s and eigenvectors v_u, v_s of the previous matrix.

```
roldan@pollo:~/research/splitting/hyper$ ./hyper
0.95387536e-3 -1.6 6                # input: mu H iterates
1.298584116092567e+00 0             # input: p^*

output:
rho_u =  2.361402084615086e+01
rho_s =  4.234772241718499e-02
v_u = ( 3.223144271056768e-03,  9.999948056570134e-01)
v_s = (-3.223144267529246e-03,  9.999948056570247e-01)
```

As a test, we compute the product of the two couples of eigenvalues. Due to symplecticity, the product should be 1 in exact computations:

```
roldan@pollo:~/research/splitting/hyper$ echo \
> '23.61402084615086*0.04234772241718499' |bc -l
.99999999994641643990
```

Notice that, due to the symmetry with respect to the horizontal, the eigenvectors should have the same entries (up to changes in sign). This is indeed true up to the 10-th digit (compare vu[0] and vs[0]).

As expected, there are two real eigenvalues

$$\rho_u = 23.61402084615086, \qquad \rho_s = 0.04234772241718499.$$

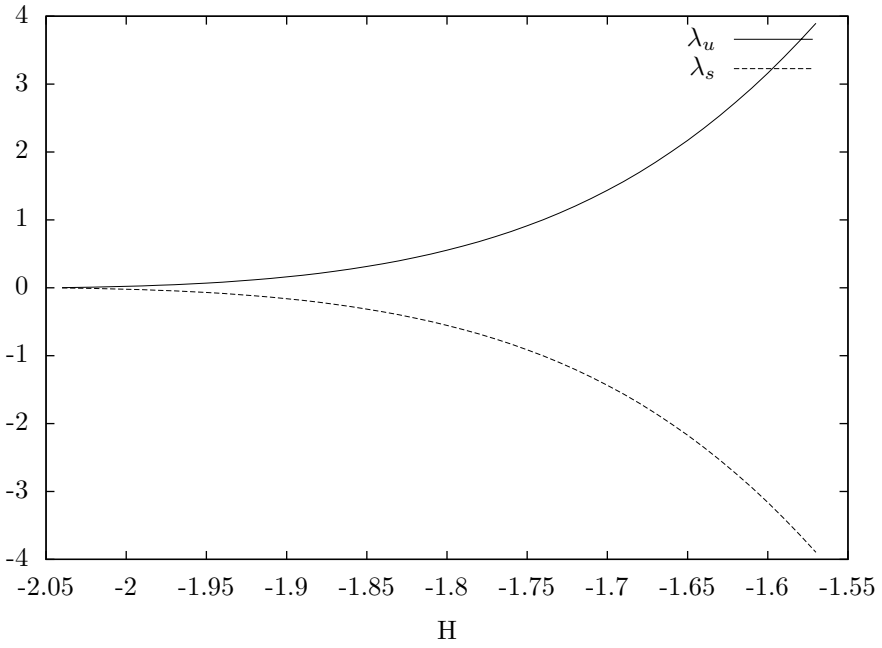

FIGURE 7. Hyperbolic splitting associated to family of periodic orbits. We plot characteristic exponents λ_u, λ_s as a function of energy level H.

The stable and unstable eigenvectors v_s, v_u (columns 1 and 2 of matrix "evects") are tangent to the stable and unstable manifolds.

Next we compute the hyperbolic splitting for the whole family of periodic orbits.

```
roldan@pollo:~/research/splitting/hyper$ ./hypers <hypers.dat
>hypers.res
```

Figure 7 shows the characteristic exponents $\lambda_u = log(\rho_u)$, $\lambda_s = log(\rho_s)$ of the periodic orbits as a function of energy H. Notice that the family loses hyperbolicity as $H \to H_-$.

4. Invariant manifolds

In this section, we compute the stable and unstable invariant manifolds associated to the periodic orbit Γ with $H = -1.6$ that we found in section 1.

Let us next compute the unstable manifold $W^u(p)$. Let h be a small displacement in the unstable direction. We will grow the manifold from the linear segment between the points $p + hv_u$ and $\mathcal{P}(p + hv_u)$. We discretize the segment into a mesh of points and iterate them by the Poincare map $\mathcal{P}$.

Points in the unstable manifold are iterated forwards by the map $\mathcal{P}$. Points in the stable manifold are iterated backwards by the *inverse* map $\mathcal{P}^{-1}$.

We compute the unstable manifold, and save it to file "unstmfld.res".

```
roldan@pollo:~/research/splitting/invmfld$ ./invmfld >unstmfld.res
0.95387536e-3 -1.6                              #input: mu, H
6                                               #input: num. iterates
1.298584116092567e+00 0                         #input: p^*
3.223144271056768e-03  9.999948056570134e-01    #input: v_u
```

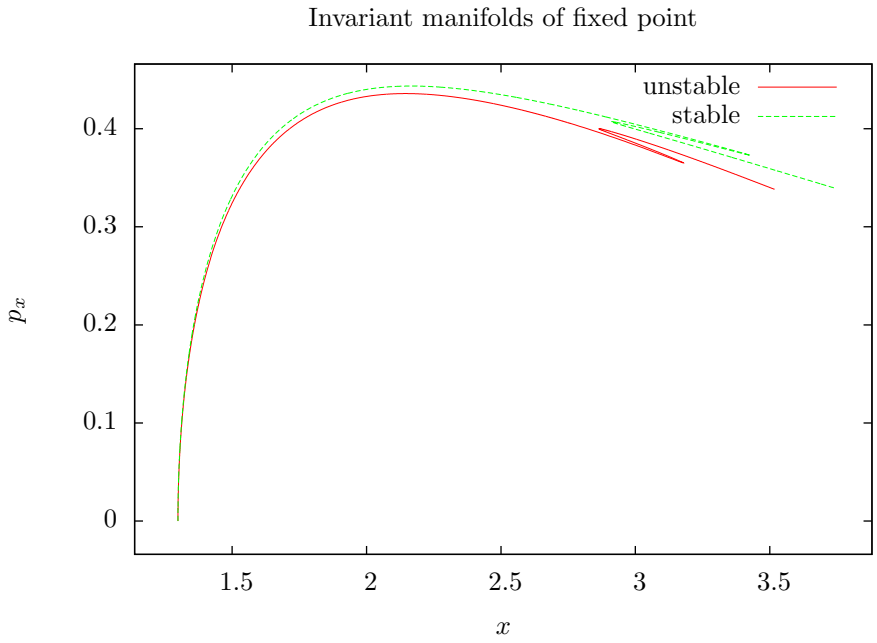

FIGURE 8. Invariant manifolds of the fixed point p^*: unstable in red, stable in green. The fixed point is located at the bottom left corner.

```
2.361402084615086e+01                          #input: rho_u
#input: desired "length" of manifold
6
0                                              #input: unstable flag

#output:
h: 1.000000e-06
Estimated error of manifold: 5.040421e-09
```

The estimated error of the manifold is computed in the following way. Let ρ_u be the unstable eigenvalue, and v_u the corresponding eigenvector. Let $\mathcal{P}$ be the Poincare map. Let p be the fixed point. If h is a small displacement in the unstable direction, then

$$\mathcal{P}(p + hv_u) = p + \rho_u h v_u + O(h^2).$$

The size of the term $O(h^2)$ can be estimated as

$$||\mathcal{P}(p + hv_u) - p - \rho_u h v_u||.$$

Similarly, in the stable case,

$$||\mathcal{P}^{-1}(p + hv_s) - p - \frac{1}{\rho_s} h v_s||.$$

Remark 4.1. In practice, we choose the small increment h such that the estimated error commited in the linear approximation of the manifold is negligible (smaller than 10^{-11}).

The unstable and stable manifolds of p^* are plotted in figure 8. Notice that both manifolds have some sharp fold. For clarity, we only grow the manifolds up to this fold. We could of course grow a longer piece of the manifolds if desired.

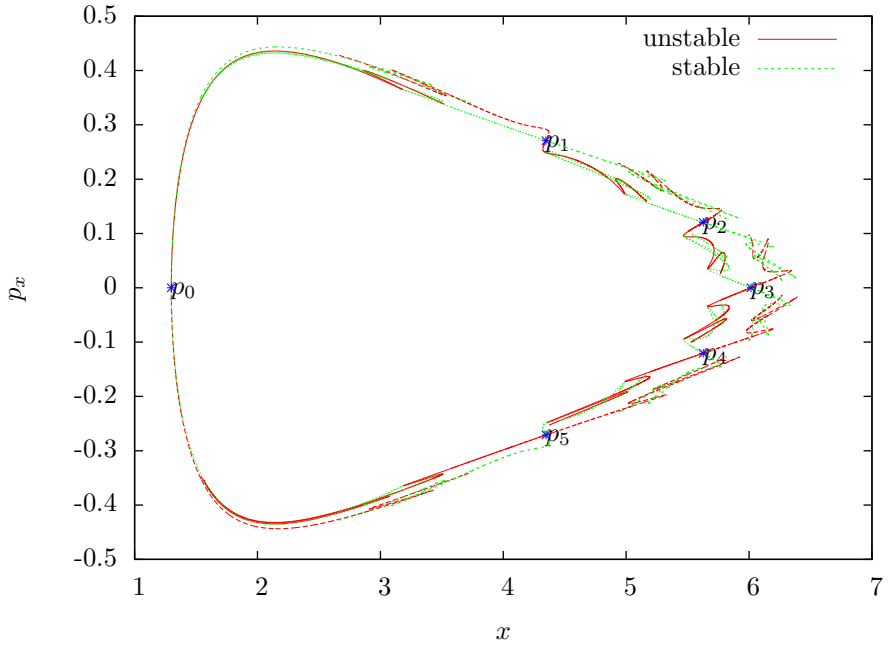

FIGURE 9. Invariant manifolds of the fixed points $p_0, p_1, \dots, p_5$. (See text). The fixed points are marked blue.

One can think of p^* as a 6-periodic point of the Poincare map P, or as a fixed point of the iterated Poincare map $\mathcal{P} = P^6$. Let $p_i = P^i(p^*)$ be the iterates of the fixed point p^*, for $i = 0, \dots, 5$. All iterates p_i are also fixed points of $\mathcal{P}$. They have associated unstable and stable manifolds, which can be obtained from $W^u(p_0), W^s(p_0)$ by iteration under P. Figure 9 shows the manifolds of all iterates.

Notice that the dynamics of the asteroid, when at perihelion, is reversible with respect to the $l = g = 0$ angles in Delaunay variables. In rotating polar variables, the condition of being at the perihelion implies $\dot r = 0$, and the $l = g = 0$ condition translates to $\phi = 0$. Hence, in rotating eucliden variables, this implies $y = 0$ and $\dot r = p_x \cos\phi + p_y \sin\phi = 0$, so $p_x = 0$.

In figure 9, it is evident that the dynamics is reversible with respect to the $p_x = 0$ line (and we have $y = 0$ because we are on the poincare section).

Figure 9 shows that the manifolds do intersect transversally at different homoclinic points. We are interested in measuring the splitting angle between the manifolds. Unfortunately, the homoclinic points do not lie on the reversibility line $p_x = 0$. This would be very useful in order to compute them.

In order to have the homoclinic points lie on the reversibility line, we look at the manifolds on the new poincare section

$$\Sigma' = \{y = 0,\ p_y < 0\}.$$

First of all, we flow the point p_0 forwards to the section Σ', obtaining a point $p_0' \in \Sigma'$.

```
roldan@pollo:~/research/splitting/prtbp2$ sec1sec2
0.95387536e-3                              #input: mu
-1.6                                       #input: H
1.298584116092567e+00 0.0                  #input: p_0
```

```
#output:
-1.600000e+00                                        # H
-3.221507692925773e+00 -3.757823611945582e-01   # p_0'
5.277795909553800e+00                                # integration time
```

Then we iterate p_0' twice to obtain p_2':

```
roldan@pollo:~/research/splitting/prtbp2$ prtbp2_2d
0.95387536e-3
-1.6
2
-3.221507692925773e+00 -3.757823611945582e-01   #input: p_0'

#output:
-5.919861224972698e+00 -5.874500915770887e-02   #output: p_2'
1.345572139790225e+01
```

Next we compute the hyperbolic splitting at p_2'.

```
roldan@pollo:~/research/splitting/hyper2$ hyper2
0.95387536e-3
-1.6
6
-5.919861224972698e+00 -5.874500915770887e-02

output:
rho_u =  2.361402083322900e+01
rho_s =  4.234772244243862e-02
v_u = (-9.945079515089161e-01, -1.046610452152056e-01)
v_s = (-9.966659836858821e-01,  8.158993175296168e-02)
```

Of course, the eigenvalues coincide with the eigenvalues previously computed on the section Σ' (see section 3).

Finally we compute the invariant manifold structure on Σ'. See figures 10 and 11. Now the points of the manifolds that lie on the symmetry line $p_x = 0$ are homoclinic points between p_2 and p_3.

Remark 4.2. By pure chance, for this energy value $H = -1.6$, the manifolds of p_2 and p_3 seem to have a secondary homoclinic tangency close to the points $(-5.67, 0.03)$ and $(-5.67, -0.03)$.

5. Homoclinic orbit

Let us now consider an energy level that is closer to the unperturbed situation, e.g. $H = -1.74$. The corresponding manifolds are given in figure 12. In this section, we compute the intersection point z of the manifolds $W^u(p_3)$ and $W^s(p_2)$.

Notice that there are two intersection points, z and $\hat{z}$, corresponding to the "inner" and "outer" separatrices, respectively. For simplicity, we will only discuss the outer separatrix; the inner one is treated analogously.

In general, there are uncountably many intersection points. For instance, in figure 11 we show 3 intersections on the symmetry line for the outer separatrix. However, in the unperturbed situation there is one distinguished intersection point located "in the middle" of the separatrix. We call it the "primary" intersection point. This corresponds to the point z in figure 12. We will continue this primary intersection into a family of intersection points $\{z_H\}$, as we vary energy.

For $H = -1.74$, the primary intersection point z corresponds to the "first" intersection of the manifolds with the $p_x = 0$ line (as we grow the manifolds from

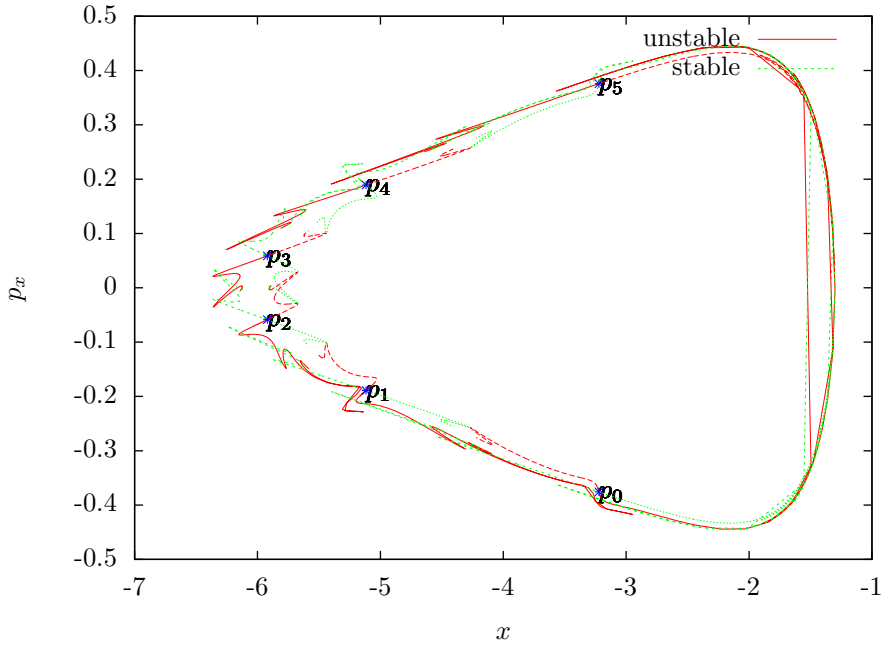

FIGURE 10. Invariant manifolds on the section Σ'.

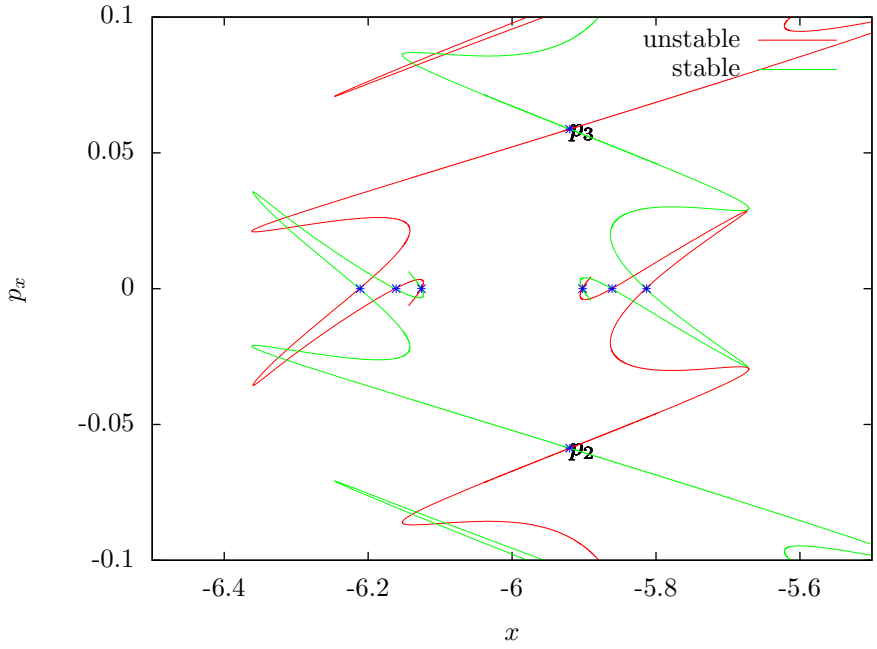

FIGURE 11. Invariant manifolds of the points p_2 and p_3 on the section Σ'. Due to the symmetry, points that lie on the line $p_x = 0$ (marked in blue) are intersection points.

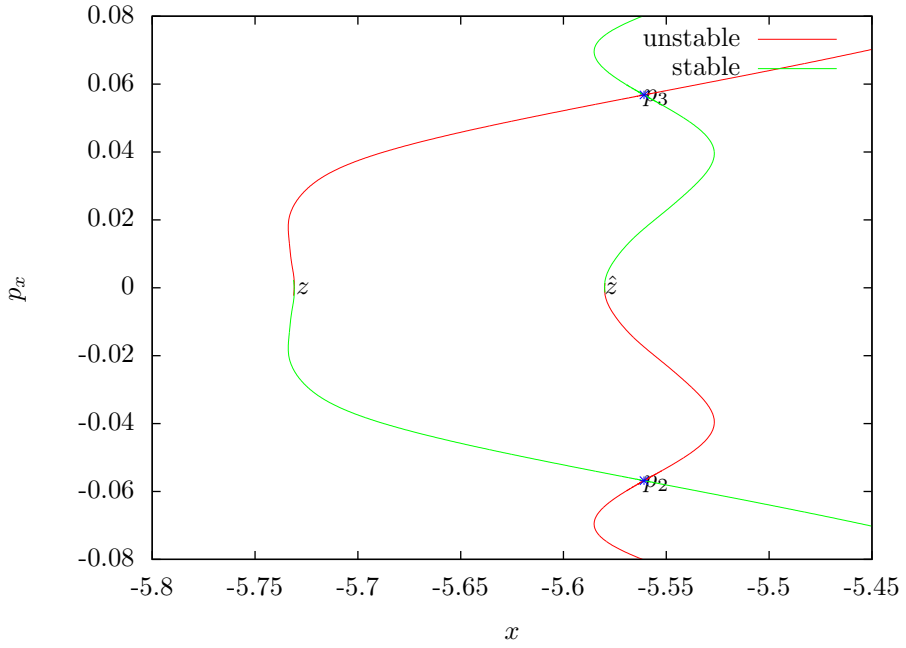

FIGURE 12. Invariant manifolds of the points p_2 and p_3 for the energy level $H = -1.74$.

the fix points). Thanks to the symmetry, it is enough to look for the intersection of $W^u(p_3)$ with the $p_x = 0$ axis, because $W^s(p_2)$ must also intersect the axis at the same point.

Let us explain the numerical method that we use to compute the homoclinic point. Let p denote the fixed point p_3' on the section Σ'. Let v_u be the unstable eigenvector associated to the point $p = p_3'$. We consider the unstable fundamental segment l_u between $p + hv_u$ and $\mathcal{P}(p + hv_u)$ defined in section 4.

First of all, we look for the first natural n such that the unstable fundamental domain $\mathcal{P}^n(l_u)$, intersects the $p_x = 0$ axis. For our example periodic orbit we need $n = 15$ iterations:

```
roldan@pollo:~/research/splitting/approxint$ approxint
#input: mu, k, unst flag, axis line
0.95387536e-3 6 0 0.0
-1.74                                                #input: H
-5.560849822624931e+00 5.681451293257738e-02         #input: p_3
-9.932197905794894e-01 -1.162516563375987e-01        #input: v_u
2.725168763316296e+00                                #input: rho_u

#output:
H: -1.740000e+00
Optimal displacement: 1.000000e-06
Estimated error of manifold: 1.267216e-12
Approximate interval: 6
Approximate splitting half-angle: 0.072504

#output:
```

```
-1.740000e+00                                          #output: H
15                                                     #output: n
#output: (h1,h2) root enclosure
1.104555663946585e-06 1.121981607929951e-06
-5.730939670475454e+00 8.640857000751058e-05   #output: z (approx)
```

Then, we use a standard numerical method (bisection-like one-dimensional root finding) to find a point p_u in the fundamental segment l_u such that

$$\pi_{p_x}(P^n(p_u)) = 0.$$

(Here, $\pi_{p_x} : \mathbb{R}^2 \to \mathbb{R}$ is the projection onto the p_x component).

```
roldan@pollo:~/research/splitting/intersec$ intersec
#input: mu, unst flag, axis line
0.95387536e-3 0 0.0
-1.74                                                   #input: H
-5.560849822624931e+00 5.681451293257738e-02    #input: p_3
-9.932197905794894e-01 -1.162516563375987e-01   #input: v_u
2.725168763316296e+00                                   #input: rho_u
15                                                      #input: n
1.104555663946585e-06 1.121981607929951e-06     #input: (h1,h2)

#output
iter =   0, [0.0000011, 0.0000011], root = 0.0000011, err(est) = 0.000000017425944
iter =   1, [0.0000011, 0.0000011], root = 0.0000011, err(est) = 0.000000007919931
...
iter =  10, [0.0000011, 0.0000011], root = 0.0000011, err(est) = 0.000000000000001
status = success
-1.740000e+00                                          #output: H
-5.560850927526564e+00 5.681438360909211e-02    #output: p_u
6.596509542858771e+02                                   #output: t_u
-5.730945639843551e+00 1.256642155700267e-10    #output: z=P(p_u)
```

Thus we obtain the homoclinic point z in figure 12. As expected, z is in the the $p_x = 0$ axis (within 10^{-10} tolerance).

Finally, we vary energy H and continue this intersection point into the family of primary intersections. We plot this family in figure 13.

Remark 5.1. Let us again consider the energy level $H = -1.6$ for a moment. Recall that in figure 11 there are 3 intersections on the symmetry line for the upper separatrix. According to figure 13, the *primary* intersection point has x coordinate equal to $x(z) = -6.12\ldots$. This corresponds to the third intersection (counting from the left) in figure 11.

6. Splitting Angle

In this section, we compute the splitting angle between the manifolds $W^u(p_3)$ and $W^s(p_2)$ at the primary homoclinic point. Again, we use the energy level $H = -1.74$ for illustrating the computations. As found in section 5, let z be the primary homoclinic point, and let p_u be the point in the unstable fundamental segment that maps to z, i.e. $\mathcal{P}^n(p_u) = z$.

Consider the tangent vector v_u to the manifold at p_u. (Recall that at this point the linear approximation is good enough, so we can take as v_u the unstable eigenvector.) Multiply v_u by the Jacobian of $\mathcal{P}$ at the successive iterates $\mathcal{P}^i(p_u)$, for $i = 0, ..., n-1$. This way, we obtain the tangent vector of the unstable manifold at z. Let us denote this vector $w_u = (w_1, w_2)$. We normalize it to $||w_u|| = 1$.

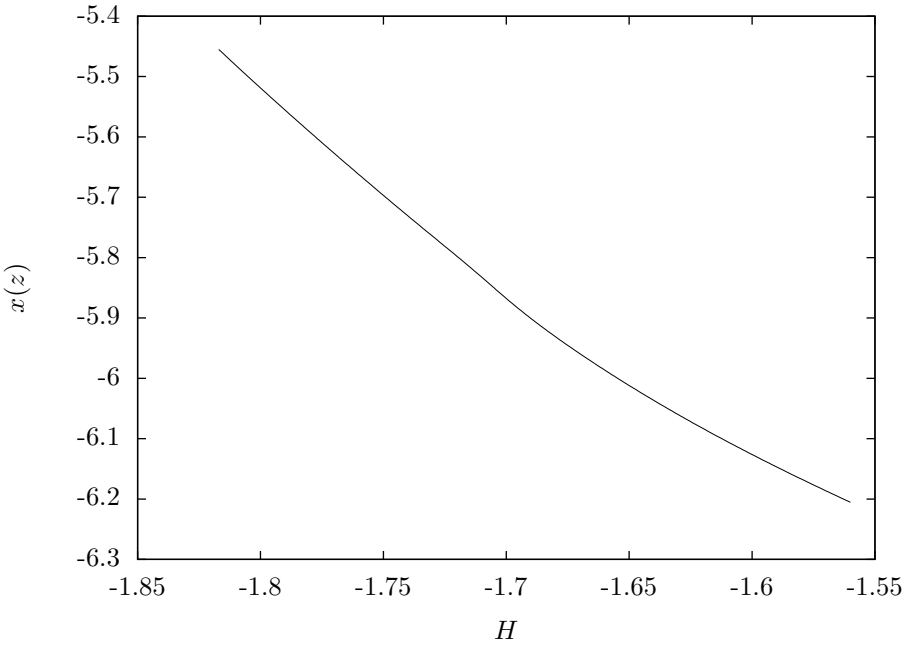

FIGURE 13. Family of primary intersection points. For each energy level H, we plot the x coordinate of the intersection point $z = (x, p_x)$ (the p_x coordinate is equal to zero). Notice that the family is continuous.

Due to reversibility, the vector tangent to the stable manifold at z is $w_s = (w_1, -w_2)$. See figure 14. Notice that we choose the tangent vectors with the appropriate orientation, i.e. with the same orientation as the trajectories on the manifolds.

Thus the oriented splitting angle between w_u and w_s is

$$\alpha = 2 \arctan_2(-w_1, -w_2),$$

where $\arctan_2$ is the arctangent function of two variables, which uses the signs of the two arguments to determine the sign of the result.

Remark 6.1. From now on, we will restrict the range of energy values to

$$H \in [-1.81, -1.56] = [H_-, H_+],$$

or equivalently the range of eccentricities to

$$e \in [0.48, 0.66] = [e_-, e_+].$$

This is the range where we can validate the accuracy of our computations (see section 6.1). Below e=0.48, splitting size becomes comparable to the numerical error. Thus one must use more sophisticated numerical methods to show that splitting is nonzero (multiple precision arithmetic, high-order approximation of local invariant manifolds using normal forms or parametrization method, etc.)

In figure 16 we plot the splitting angle associated to the outer separatrix for $e \in [e_-, e_+]$ (in green). The splitting angle is nonzero for all energy values except for a discrete set. The splitting angle oscillates around zero with decreasing amplitude as $e \to e_-$.

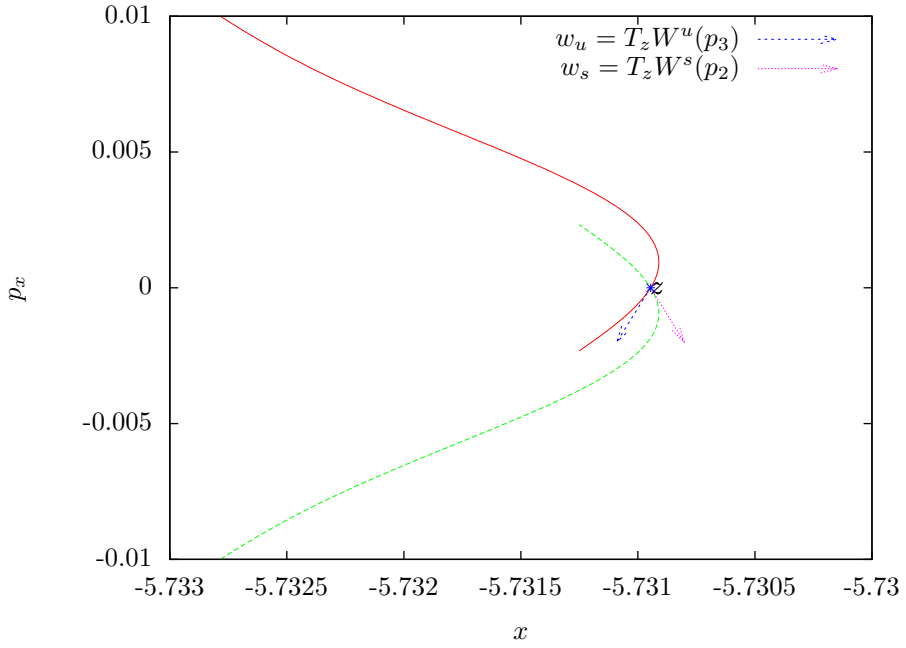

FIGURE 14. Magnification of figure 12 at the intersection point z. We show the vectors w_u, w_s tangent to the unstable and stable manifolds at z. Splitting angle α is the angle between w_u and w_s.

Numerically, we find that the zeros of the splitting angle are contained in the intervals listed in table 2 (right column).

*** We could study the behavior of α to see how exactly how fast does it decrease: as a power, as en exponential? ***

6.1. **Accuracy of the Computations.** For small eccentricities, the splitting angle α becomes very small. We need to check the validity of α, making sure that the size of (accumulated) numerical errors in the computation is smaller than the size of α.

The smallest splitting angle in figure 16, corresponding to $e = 0.48$, is

$$\alpha(0.48) = -1.777970294158603 \times 10^{-5}.$$

We check the validity of $\alpha(0.48)$ by recomputing this angle using an alternative numerical method. First we compute the intersection of the manifolds $W^u(p_3)$ and $W^s(p_2)$ with the horizontal axis defined by

$$p_x = \frac{j}{10^5}$$

for $j \in (-2, -1, 1, 2)$.

In table 1 we tabulate the x coordinate of $W^u(p_3)$ and $W^s(p_2)$ on these axis, and their difference $d = x^u - x^s$ gives the distance between the manifolds. We apply numerical differentiation to the last column of this table, using central differences centered at z with step sizes 0.00002 and 0.00004, and obtain the values:

$$d1 = \frac{d(0.00001) - d(-0.00001)}{0.00002} = -0.0000177691.$$

p_x	x^u	x^s	$x^u - x^s$
-0.00002	-5.481541931871417	-5.481541932226887	0.000000000355470
-0.00001	-5.481541931790012	-5.481541931967703	0.000000000177691
0.00000	-5.481541931822124	-5.481541931822124	0.000000000000000
0.00001	-5.481541931967703	-5.481541931790012	-0.000000000177691
0.00002	-5.481541932226887	-5.481541931871417	-0.000000000355470

TABLE 1. Sampling of the manifolds $W^u(p_3)$ and $W^s(p_2)$ at different values of p_x, and their difference (last column).

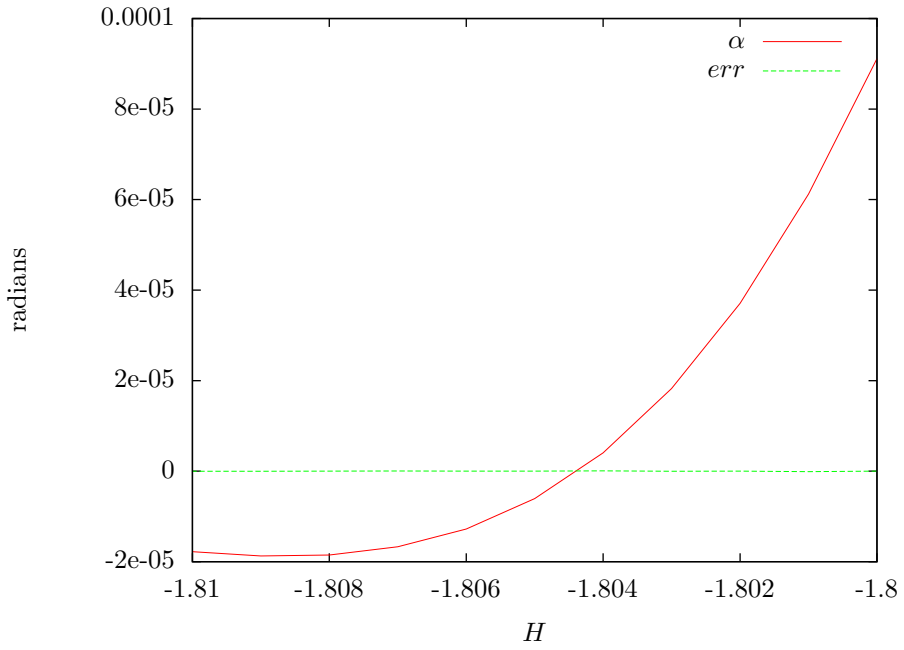

FIGURE 15. Splitting angle $\alpha(H)$ and estimate of the numerical error $err(H)$ as a function of energy level H.

$$d2 = \frac{d(0.00002) - d(-0.00002)}{0.00004} = -0.0000177735.$$

Finally, we use Richardson extrapolation and obtain:

$$d = \frac{4d1 - d2}{3} = -0.00001776763333333333.$$

Thus, using this second method, we obtain the splitting angle

$$\alpha(0.48) = atan(-0.00001776763333333333) = -0.00001776763333146364.$$

Compare the splitting angle computed using the two methods. They differ by approximately 10^{-8}. This gives an estimate of the numerical error commited in our computation of the splitting angle.

We repeat this test for a range of energies $H \in [-1.81, -1.8]$. In figure 15, we compare the splitting angle $\alpha(H)$ and the estimate of the numerical error $err(H)$. This error stays below 10^{-7}, and it is several orders of magnitude smaller than the splitting angle. Therefore we are confident that the splitting angle has been accurately computed in the range of eccentricities considered, $[e_-, e_+] = [0.48, 0.66]$.

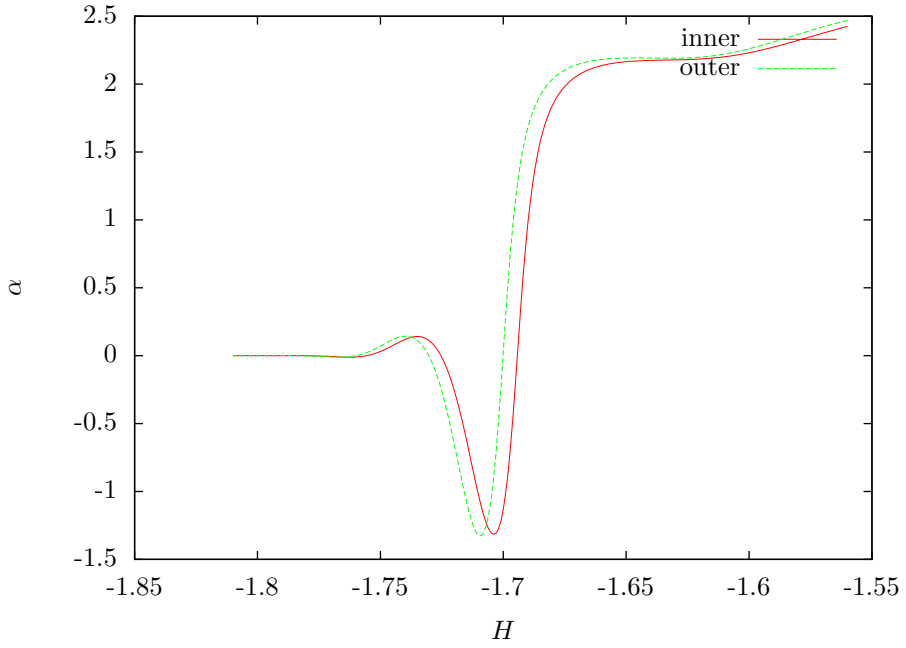

FIGURE 16. Splitting angle associated to inner and outer separatrices (in radians).

inner	outer
$(-1.695, -1.694)$	$(-1.701, -1.700)$
$(-1.726, -1.725)$	$(-1.731, -1.730)$
$(-1.756, -1.755)$	$(-1.760, -1.759)$
$(-1.781, -1.780)$	$(-1.784, -1.783)$
$(-1.802, -1.801)$	$(-1.805, -1.804)$

TABLE 2. Intervals containing the zeros of inner splitting (left column) and outer splitting (right column).

7. Inner splitting

Finally, let us consider the family of primary homoclinic intersections $\hat{z}_H$ associated to the *inner* separatrix. Proceeding in the same way as in sections 5 and 6, we compute the splitting angle associated to the inner separatrix.

The inner and outer splittings are very similar. See figure 16. However, they become zero at different values of H. See table 2.

8. Delaunay coordinates

We have programmed the transformation to obtain rotating Delaunay coordinates (l, L, g, G) from rotating cartesian (x, y, p_x, p_y). For example, let us transform the fixed point p_0 corresponding to periodic orbit with $H = -1.6$.

```
roldan@pollo:~/research/splitting/cardel$ ./cardel
0.95387536e-3                                        #input: mu
-1.6                                                 #input: H
1.298584116092567e+00 0 0 1.124715918064501e+00   #input: (x,y,p_x,p_y)
```

```
#output: (l,L,g,G)
0.000000000000000e+00 1.906394680726033e+00       # l, L
0.000000000000000e+00 1.460538226315030e+00       # g, G
```

Since p_0 is at the perihelion when $t = 0$, it has Delaunay coordinates $l = g = 0$.

Next we have programmed the vector field of the RTBP in Delaunay coordinates.

*** Write down equations of RTBP in Delaunay coordinates. These are quite cumbersome expressions! Moreover, we have to deduce eccentricy u numerically. Also, there is a trick by Vadim to determine the sign of u. ***

For instance, we compute the vector field at the fixed point p_0 corresponding to the periodic orbit with $H = -1.6$.

```
roldan@pollo:~/research/splitting/rtbp_del$ ./rtbpdel
0.95387536e-3                                     #input: mu
#input: p_0
0.000000000000000e+00 1.906394680726033e+00   # l, L
0.000000000000000e+00 1.460538226315030e+00   # g, G

#output: d/dt(l,L,g,G)
1.408489723196100e-01 -0.000000000000000e+00  #d/dt(l,L)
-9.791011070652882e-01 -0.000000000000000e+00 #d/dt(g,G)
```

Since p_0 is at the perihelion when $t = 0$, the derivatives of L (square of semimajor axis) and G (angular momentum) are zero.

To test the correctness of the vectorfield, we compare each component to the corresponding partial derivative of the Hamiltonian function. The partial derivative is computed numerically using a central differences squeme.

```
roldan@pollo:~/research/splitting/rtbp_del$ ./rtbpdel_test
0.95387536e-3                                     #input: mu
#input: p_0
0.000000000000000e+00 1.906394680726033e+00   # l, L
0.000000000000000e+00 1.460538226315030e+00   # g, G

#output: numerical derivatives versus analytical derivatives
L = 1.906395e+00
dot l = H'(L) = 0.1408489720 +/- 0.0000000235 # numerical
dot l = y[0] = 0.1408489723                   # analytical

l = 0.000000e+00
dot L = -H'(l) = 0.0000000002 +/- 0.0000000215
dot L = y[1] = -0.0000000000

G = 1.460538e+00
dot g = H'(G) = -0.9791011052 +/- 0.0000000262
dot g = y[2] = -0.9791011071

g = 0.000000e+00
dot G = -H'(g) = -0.0000000008 +/- 0.0000000221
dot G = y[3] = -0.0000000000
```

Notice that the difference between the analytical and numerical derivatives is smaller than the estimated numerical error (written after the $\pm$ sign).

Next we have programmed the flow of the RTBP in Delaunay coordinates. For example, we compute the flow at the periodic point p_0 after time $T = 44.01796898996710$ (the period of the periodic orbit, as computed in section 1).

```
roldan@pollo:~/research/splitting/frtbp_del$ frtbpdel
#input:
0.95387536e-3
44.01796898996710
0.000000000000000e+00 1.906394680726033e+00
0.000000000000000e+00 1.460538226315030e+00

#output:
6.283185307179695e+00 1.906394680725900e+00
-4.398229715025703e+01 1.460538226315012e+00
```

Since this is a periodic orbit, the final condition has coords

$$\Phi_T(p_0) = (l = 2\pi,\ L,\ g = -14\pi,\ G).$$

Finally, consider the poincare section

$$\Sigma_g = \{g = 0\},$$

and let $P_g \colon \Sigma_g \to \Sigma_g$ be the associated Poincare map. Equivalently, if g was considered as "time", P_g would be the time-2π map, or stroboscopic map. Notice that, in the rotating Delaunay variables, a $7:1$ resonant periodic orbit crosses the section Σ_g precisely 7 times.

For example, we compute the 7-th iterate of p_0 under the poincare map P_g.

```
roldan@pollo:~/research/splitting/prtbp_del$ ./prtbpdel
0.95387536e-3 7                                  #input: mu, iterates
#intpu: p_0
0.000000000000000e+00 1.906394680726033e+00   # l, L
0.000000000000000e+00 1.460538226315030e+00   # g, G

#output: P_g^{7}(p_0)
9.947598300641403e-14 1.906394680725914e+00   # l, L
0.000000000000000e+00 1.460538226315020e+00   # g, G
4.401796898996748e+01                          # integration time
```

Since this is a periodic orbit, the final condition has coords

$$P_g^7(p_0) = (l = 2\pi,\ L,\ g = -14\pi,\ G).$$

Notice that the period of the periodic orbit $T = 44.017\ldots$ agrees with the one computed in section 1 using euclidean coordinates.

Similarly, we can compute the inverse poincare map P_g^{-1}.

9. Resonance structure

To better describe the resonance structure, we plot the manifolds using Delaunay variables. Consider the fixed point p_0 corresponding to the periodic orbit with $H = -1.6$.

First, we obtain the unstable and stable invariant manifolds of the point p_0, and transform them to Delaunay variables. Notice that the transformed invariant manifolds do not lie on the $\Sigma_g = \{g = 0\}$ section. Thus we apply the Delaunay flow to each point in the invariant manifolds until it lies on the Σ_g section.

To obtain the manifolds of all fixed points, We iterate the invariant manifolds of p_0 by the Poincare map P_g 7 times.

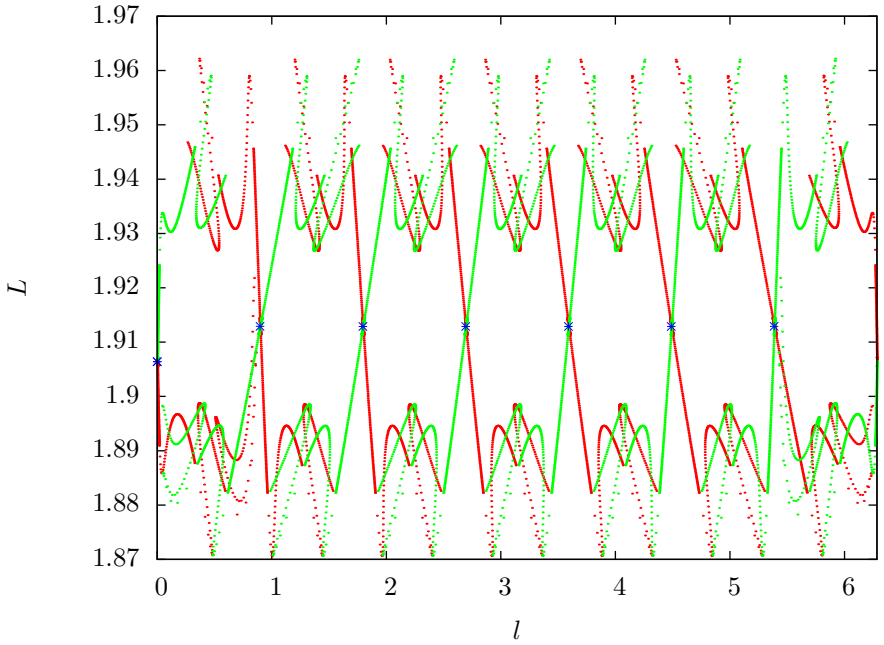

FIGURE 17. Invariant manifolds in Delaunay variables.

```
roldan@pollo:~/research/splitting/doc/figs$ ./orbitpdel
<unstmfld_it0.dat >unstmfld_it0.res
```

Figures 17 and 18 show the manifolds in Delaunay variables, on the Σ_g section. The manifolds "look like" those of a perturbed pendulum.

The fixed points p_0, p_1, ..., p_6 are *almost* (but not exactly) equidistributed on the l axis. This is natural since the $\mu = 0$ circular resonant periodic orbit crosses the $\Sigma_0 = \{g = 0\}$ section every $l = 2\pi k/14$ for $k = 0, \ldots, 6$.

Similarly, the invariant manifold structure is almost (but not exactly) repeated every $2\pi/7 = 0.897\ldots$.

The manifold structure is symmetrical with respect to the vertical lines $l = 0$ and $l = \pi$.

*** TO DO ***

We should also plot the resonant periodic orbit that we studied in the beginning of this work. The associated manifolds look like a figure-eight inside the pendulum.

*** TO DO ***

10. Reduced flow of the circular problem

The program *frtbpred* computes the time-s reduced flow of the circular problam. As a test, we integrate the initial condition corresponding to the periodic orbit for time exactly $s = 14\pi$.

```
roldan@pollo:~/research/splitting/frtbp_red$ frtbpred
0.95387536e-3
43.98229715025710533816                        # input: int.time s=14\pi
# input: initial condition x=(l,L,g,G,t,I)
0.000000000000000e+00 1.906394680726033e+00
0.000000000000000e+00 1.460538226315030e+00
```

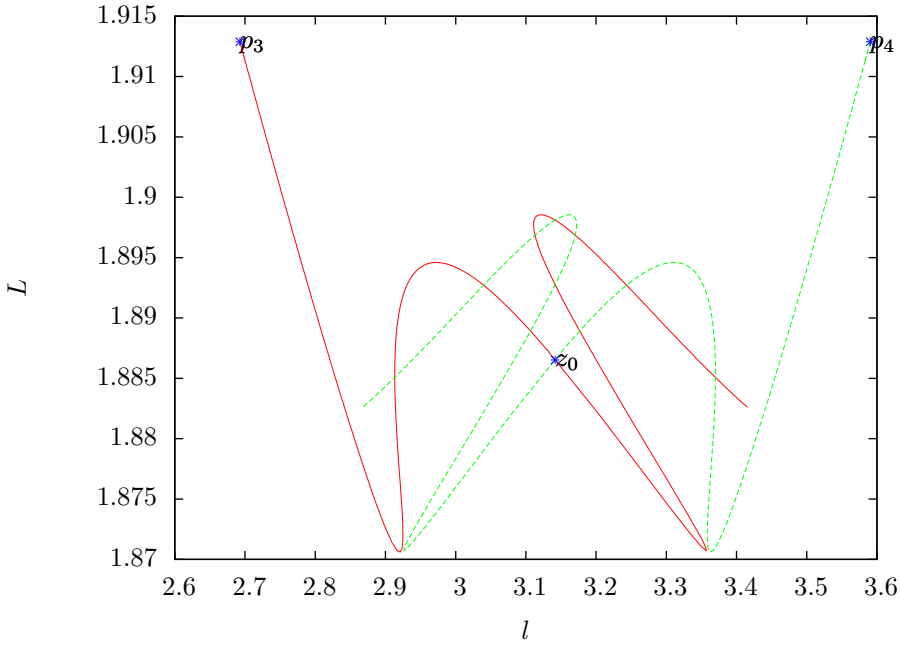

FIGURE 18. Invariant manifolds in Delaunay variables (zoom).

```
0 0

# output: final condition \phi(s,x)=(l,L,g,G,t,I)
-6.283185307179716e+00 1.906394680725890e+00
4.398229715025710e+01 1.460538226315010e+00
-4.401796898996715e+01 0.000000000000000e+00
```

As expected, the final condition has coords

$$\phi(s,x) = (l = -2\pi,\ L,\ g = 14\pi,\ G,\ t = -(14\pi + \mu T_0),\ I).$$

In particular, note that t coincides with the period of the periodic orbit in the old time.

11. Inner and outer dynamics of the circular problem

11.1. **Inner dynamics.** For the circular problem, the invariant cylinder is foliated by periodic orbits. According to Marcel's notes, the inner map for the circular problem is given by

$$F_0^{in}\colon\ (I,t) \to (I, t + \mu T_0(I)).$$

Here, $\mu T_0(I)$ is the period of the periodic orbit (modulo 2π) in the original time t. Recall that we computed the periodic orbit as well as its period in section 1.3. We plot the period $\mu T_0(H)$ as a function of energy level H in figure 19.

The derivative of the function $\mu T_0(H)$ is clearly nonzero. This means that the inner map is twist (and thus one can apply KAM theorem).

As an extra test, we compute the same shift μT_0 for a specific energy level $H = -1.6$ using two different methods. First by computing the period of the periodic

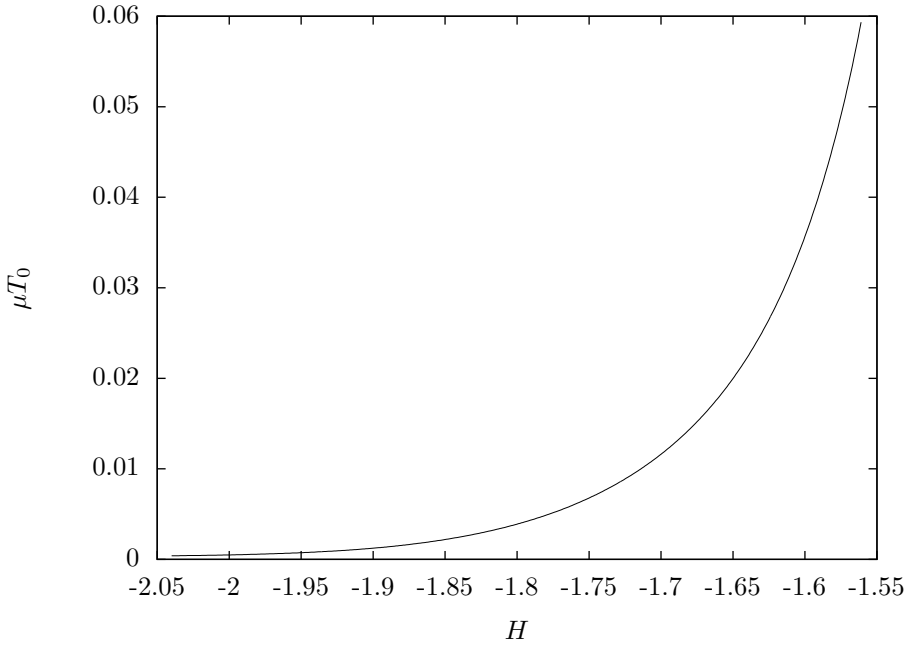

FIGURE 19. Shift μT_0 of the inner map, as a function of energy level H.

orbit. The period was computed in section 1.3, and it is $2 \times 2.200898449498355e+01 = 4.401796898996710e+01$. Thus the shift is

$$\mu T_0(-1.6) = 44.01796898996710e+01 \mod 14\pi = .03567183970999466184.$$

Then by computing the integral expression in Marcel's notes using numerical integration:

```
roldan@pollo:~/research/splitting/inner_circ$ ./inner_circ <inner_circ.dat

# output:
estimated error =  5.347e-13
3.567183971001953e-02           # \mu T_0
```

The difference in computing the shift using both methods is of the order 10^{-10}.

11.2. **Outer dynamics.** According to Marcel's notes, the outer map for the circular problem is given by

$$F_0^{out}\colon\ (I,t) \to (I, t + \mu\omega_0(I)),$$

where

$$\omega_0(I) = -\omega_0^-(I) - \omega_0^+(I).$$

Let us explain how we compute ω_0^+. Fix $(H_0 = -1.74, t_0 = 0)$, that is the level of energy and initial condition in t. Recall that in section 5 we obtained a primary homoclinic point which belongs to the Poincare section Σ'.

We transform this homoclinic point from Cartesian variables to Delaunay. From now on, we work with the reduced flow in Delaunay coordinates for the circular problem.

```
roldan@pollo:~/research/splitting/cardel2$ cardel2_2d
0.95387536e-3                                  #input: mu
-1.74                                          #input: H
-5.730945639853097e+00 0                       #input: z=(x,p_x)

#output: z=(l_h, L_h, g_h, G_h)
3.141592653589793e+00 1.922442586446909e+00  # l_h, L_h
6.283185307179586e+00 1.604706451008939e+00  # g_h, G_h
```

Notice that, due to reversibility, the homoclinic point has $g_h = 2\pi = 0$, so it is precisely on the section $g = 0$. THIS IS PERFECT, because we don't need to flow it forwards until it reaches the section $g = 0$.

We would like to take the extended point $(l_h, L_h, 0, G_h, t_0)$ and flow it from $s = 0$ until $s = 14N\pi$, for a certain (big) natural N. Then we would obtain a new point $(l_h^+, L_h^+, 0, G_h^+, t_1)$ which is very close to the cylinder.

Numerically, however, forward integration along the stable manifold leads to amplification of errors. In practice, we arrange this computation as backward integration. We consider the point p_u that we found in section 5. Recall that p_u is in the unstable manifold of the non-reduced flow, very close to the cylinder. Equivalently, it is in the *stable* manifold for the reduced flow. Thus let us rename the point by p_s. Notice that p_s is not in the section $g = 0$.

```
roldan@pollo:~/research/splitting/cardel2$ cardel2_2d
0.95387536e-3
-1.74
-5.560872184178592e+00 5.681189561885759e-02   #input: p_s = (x,p_x)

#output: p_s=(l,L,g,G)
3.614415602587796e+00 1.912860780992552e+00    # l, L
6.115377037688049e+00 1.603347301832497e+00    # g, G
```

We flow p_s backwards (by the reduced flow) until it reaches the section $g = 0$. Thus, we obtain a different point, with coordinates $(l_h^+, L_h^+, 0, G_h^+)$, that is close to p_s. Take the extended point $(l_h^+, L_h^+, 0, G_h^+, t_0)$ and flow it *backwards* from $s = 0$ until $s = -14N\pi$, for a certain (big) natural N. Then we obtain the homoclinic point $(l_h, L_h, 0, G_h, -t_1)$ in the section $g = 0$.

Remark 11.1. We take t_1 modulo 2π.

As explained in Marcel's notes, from the definition of the inner map it follows that $t_2 = t_1 + N\mu T_0$. Finally, the function ω_0^+ is simply $\omega_0^+ = t_2 - t_0$.

Analogously, we can find ω_0^-.

As a test, we consider a fixed value of energy $H = -1.6$, and we compute the value of ω_0 for different number of iterates N. See figure 20. As expected, ω_0 has order μ, and it converges to an asymptotic value as N increases.

Finally, we compute ω_0 as a function of energy H. The result is shown in figure 21.

A helpful test to verify that the function ω_0^+ is correct is to check that indeed, the homoclinic orbit and the periodic orbit converge

$$dist^+(s) \equiv |\Phi_s(l_h, L_h, 0, G_h, t_0) - \Phi_s(l_p, L_p, 0, G_p, t_0 + \omega_0^+)| \xrightarrow{s\to\infty} 0$$

with exponential decay. We have performed this test for values of the energy in the range $[-1.74, -1.56]$.

The result of the test is shown in figure 22. Notice that the vertical axis is in logarithmic scale. Let $s = 14N\pi$. We plot the function $dist^+$ as a function of N (multiples of the period). The test shows exponential decay of the distance function

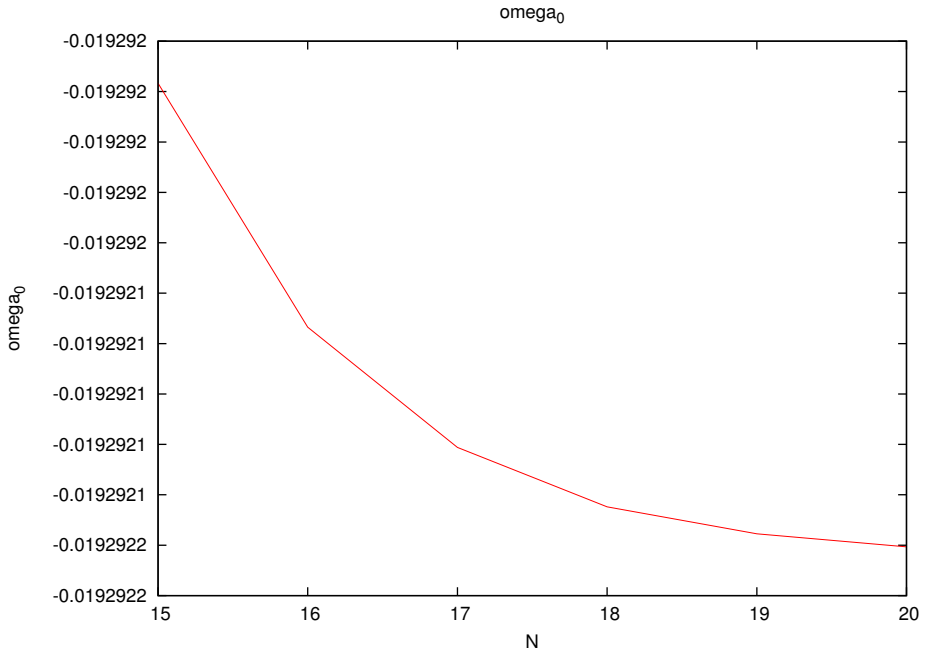

FIGURE 20. Convergence of ω_0 as a function of the number of iterates N along the homoclinic orbit.

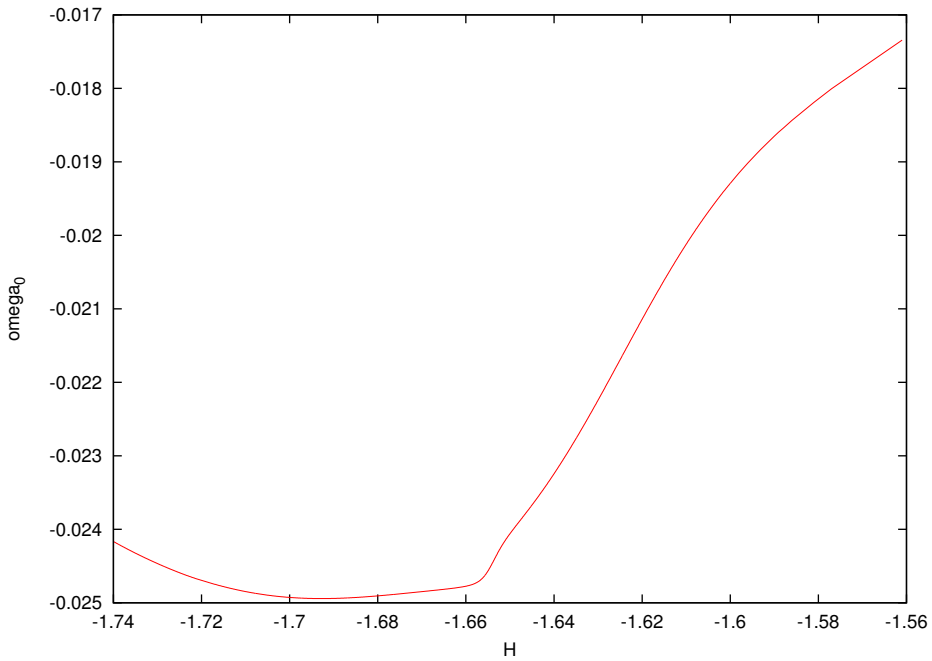

FIGURE 21. Shift ω_0 of the outer map, as a function of energy level H.

for $s \leq 14 \cdot (14\pi) \approx 600$. For most energies, there is exponential decay up to time $s = 20 \cdot (14\pi) \approx 880$.

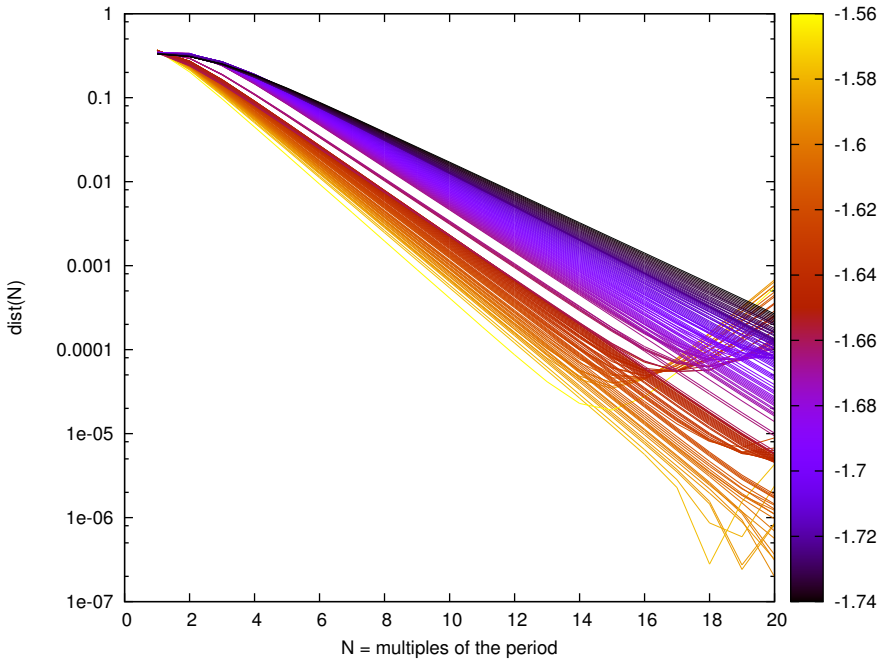

FIGURE 22. Exponential decay of the function $dist^+$ as a function of N (multiples of the period) for different energy levels $H \in [-1.74, -1.56]$.

Recall that the periodic orbit becomes more hyperbolic as energy H increases. Thus, the rate of exponential convergence between the homoclinic orbit and periodic orbit increases as H increases. This is in accordance to figure 22.

We have also performed the same test for ω_0^-, and we have verified that

$$dist^-(s) \equiv |\Phi_s(l_h, L_h, 0, G_h, t_0) - \Phi_s(l_p, L_p, 0, G_p, t_0 - \omega_0^-)| \xrightarrow{s\to-\infty} 0$$

with exponential decay.

12. Inner and outer dynamics of the elliptic problem

12.1. **Inner dynamics.** We study the inner map of the elliptic problem. From Marcel's notes, we want to compute the first order of the I component

$$A_1(I,t) = A_1^+(I,t)e^{it} + A_1^-(I,t)e^{-it}.$$

Since A_1^+ and A_1^- are complex conjugate,

$$A_1(I,t) = 2\Re(A_1^+)\cos(t) - 2\Im(A_1^+)\sin(t).$$

Let us define the complex function

$$f(l,L,g,G) = \frac{\partial_t \Delta H_{ell}^{1,+}(l,L,g,G)}{-1 + \mu\partial_G \Delta H_{circ}(l,L,g,G)}. \tag{4}$$

We need to compute the complex integral $A^+(I)$ in Marcel's notes

$$A^+(I) = -\mu \int_0^{-14\pi} f(\Phi_s(l_p, L_p, 0, G_p))e^{it(s)}ds,$$

where Φ_s denotes the flow of the reduced system, and $(l_p, L_p, 0, G_p)$ is the periodic point on the section $g = 0$.

Notice that the denominator of f is the same one used for the inner dynamics of the circular problem. Next we compute the numerator explicitly. Let

$$\Delta H^1_{ell}(l,L,g,G,t) = \frac{1-\mu}{\mu^2} B_1(-\frac{r}{\mu}, v, g-t, t) - \frac{1}{1-\mu} B_1(\frac{r}{1-\mu}, v, g-t, t), \tag{5}$$

where

$$B_1(r,v,g-t,t) = -\frac{1}{2\Delta^3(r,v,g)}(2\cos t - 3r\cos(v+g+t) + r\cos(v+g-t)),$$
$$\Delta(r,v,g) = (r^2+1-2r\cos(v+g))^{1/2}.$$

Remark 12.1. In equation (5), we follow Marcel and Vadim's convention to place the large mass (Sun) to the left of the origin, and the small mass (Jupiter) to the right. In the code, however, we follow the astrodynamics convention to place the large mass (Sun) to the right of the origin, and the small mass (Jupiter) to the left. The only difference would be the terms $B_1(\frac{r}{\mu}, v, g-t, t)$ and $B_1(-\frac{r}{1-\mu}, v, g-t, t)$. We should probably stick to one convention.

We write B_1 as a sum of harmonics

$$\begin{aligned} B_1(r,v+g,t) &= -\frac{1-r\cos(v+g)-i2r\sin(v+g)}{2\Delta^3(r,v+g)}e^{it} - \frac{1-r\cos(v+g)+i2r\sin(v+g)}{2\Delta^3(r,v+g)}e^{-it} \\ &\equiv B_1^+(r,v+g)e^{it} + B_1^-(r,v+g)e^{-it}. \end{aligned}$$

Thus we have

$$B_1^+(r,v+g) \equiv -\frac{1-r\cos(v+g)-i2r\sin(v+g)}{2\Delta^3(r,v+g)}.$$

Taking partial derivatives with respect to t we obtain

$$\partial_t \Delta H^1_{ell} = \frac{1-\mu}{\mu^2}\partial_t B_1(-\frac{r}{\mu}, v, g-t, t) - \frac{1}{1-\mu}\partial_t B_1(\frac{r}{1-\mu}, v, g-t, t),$$

with

$$\partial_t B_1(r,v+g,t) = iB_1^+(r,v+g)e^{it} - iB_1^-(r,v+g)e^{-it}.$$

Putting it all together,

$$\begin{aligned} \partial_t \Delta H^1_{ell} &= \frac{1-\mu}{\mu^2}\left[iB_1^+(-\frac{r}{\mu}, v+g)e^{it} - iB_1^-(-\frac{r}{\mu}, v+g)e^{-it}\right] \\ &\quad - \frac{1}{1-\mu}\left[iB_1^+(\frac{r}{1-\mu}, v+g)e^{it} - iB_1^-(\frac{r}{1-\mu}, v+g)e^{-it}\right] \\ &\equiv \partial_t \Delta H^{1,+}_{ell} e^{it} + \partial_t \Delta H^{1,-}_{ell} e^{-it}. \end{aligned}$$

Therefore we have

$$\partial_t \Delta H^{1,+}_{ell} = \frac{1-\mu}{\mu^2} iB_1^+(-\frac{r}{\mu}, v+g) - \frac{1}{1-\mu} iB_1^+(\frac{r}{1-\mu}, v+g).$$

Figure 23 shows the complex integral A^+. We plot its real part, imaginary part, and its modulus, as a function of energy level H.

12.2. **Outer dynamics.** We need to compute the complex integral $\Omega^+(I)$ in Marcel's notes

$$\Omega^+(I) = -B^+(I) - C^+(I),$$

where

$$B^+(I) = -\mu \int_0^{14M\pi} f(\Phi_s(x_h)))e^{it(s)} - f(\Phi_s(x_p))e^{i(t(s)+\omega_0^+)}ds,$$

$$C^+(I) = -\mu \int_{-14M\pi}^0 f(\Phi_s(x_h))e^{it(s)} - f(\Phi_s(x_p)e^{i(t(s)-\omega_0^-)}ds.$$

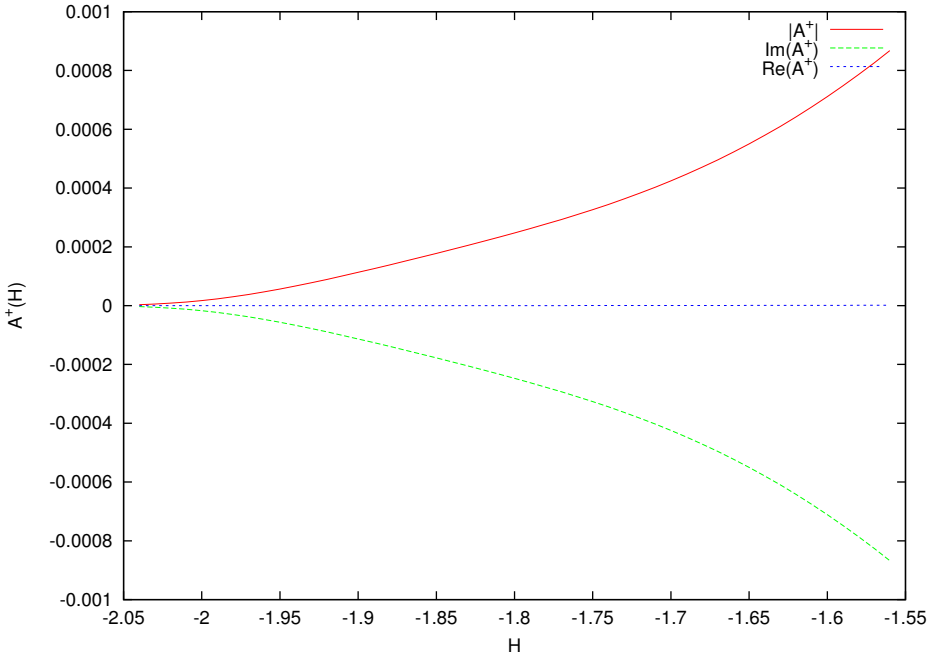

FIGURE 23. The complex integral A^+, as a function of energy level H.

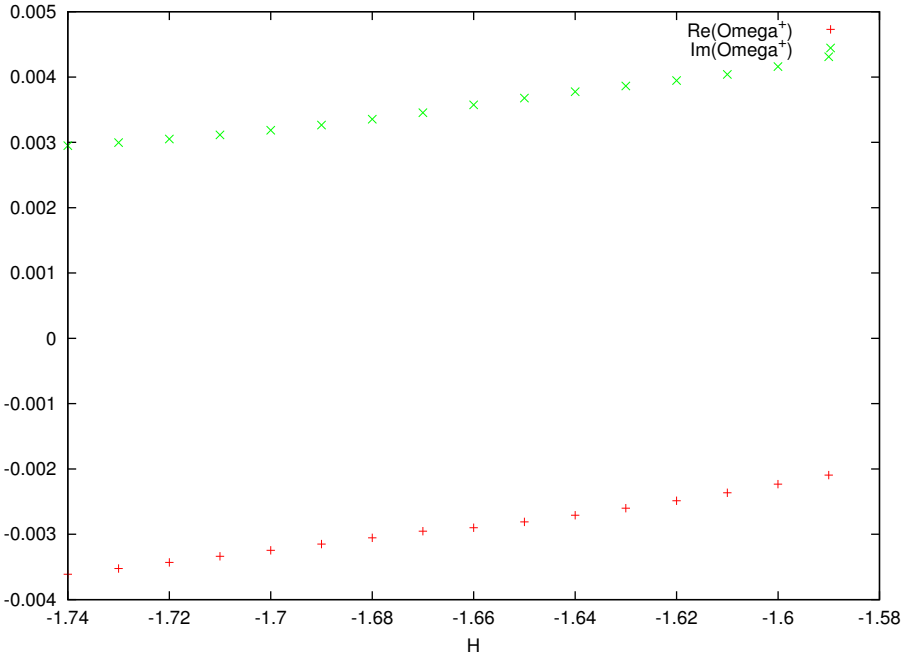

FIGURE 24. The complex integral Ω^+, as a function of energy level H.

where Φ_s denotes the flow of the reduced system, and x_h, x_p are the homoclinic and periodic points in the $g = 0$ section.

Figure 24 shows the complex integral Ω^+. We plot its real part and imaginary part as a function of energy level H.

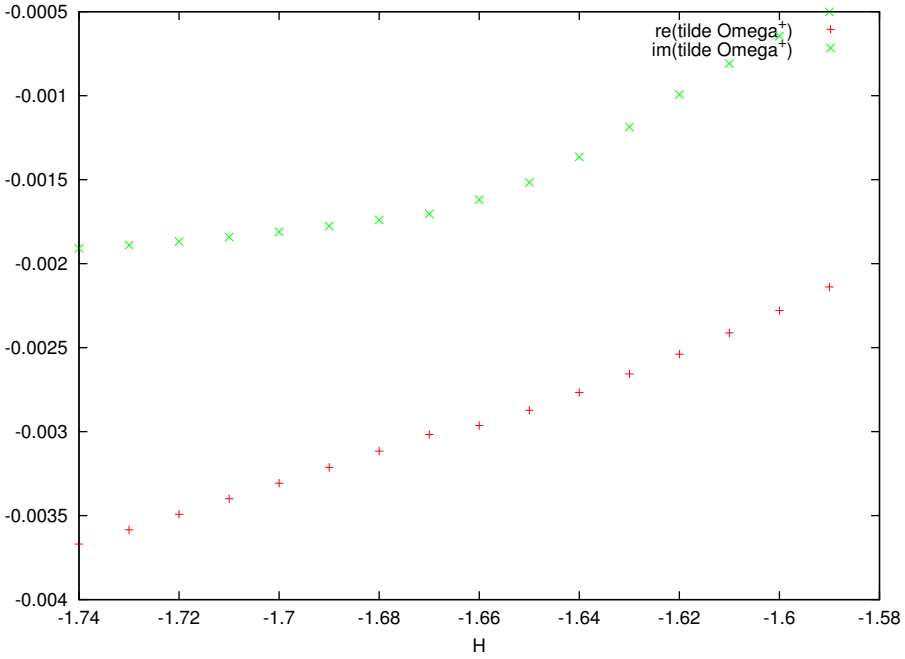

FIGURE 25. The complex integral $\tilde{\Omega}^+$, as a function of energy level H.

13. Absence of common invariant curves

To see that there are no common invariant curves it is enough to check that the function //

$$\tilde{\Omega}^+(I) = \Omega^+ - \frac{e^{i\omega_0} - 1}{e^{iT_0} - 1} A_1^+$$

is non-zero for a range of energies, where

- T_0 is related to the inner map of the circular problem, and is computed in program "periods".
- ω_0 is related to the outer map of the circular problem, and is computed in program "omega".
- A_1^+ is related to the inner map of the elliptic problem, and is computed in program "inner_ell".
- Ω^+ is related to the outer map of the elliptic problem, and is computed in program "outer_ell".

Figure 25 shows the complex integral $\tilde{\Omega}^+$. We plot its real part and imaginary part as a function of energy level H. Therefore, we see that indeed there are no common invariant curves.

14. Connecting resonant 7:1 and 8:1 orbits

Following Vadim's suggestion, we check to see if there is heteroclinic connection between the periodic orbit $\Gamma_{7:1}$ with period $T_{7:1} \approx 14\pi$, and the periodic orbit $\Gamma_{8:1}$ with period $T_{8:1} \approx 16\pi$.

As before, we will compute the periodic orbits, their hyperbolic invariant manifolds, and check if they intersect.

We look for these two periodic orbits in the same level of energy $H = -1.6$. Notice that in section 1 we used a slightly different value $H = H_0$ (see equation (2)).

We start by obtainig an approximation to the periodic orbits from the 2BP. I have written a simple script that, given a resonance, returns the initial condition at the perihelion corresponding to that resonant periodic orbit in the 2BP.

```
roldan@pollo:~/research/splitting$ bc -l initcond.bc
Resonance (p/q, p=period of Asteroid, q=period of Jupiter)? 7/1
G = 1.46336205837340077849      # output: angular momentum
e = .64404909086496709969       # output: eccentricity
Initial condition at perihelion (in euclidean coords):
x = 1.30253319428569378555      # output: x
v_y = 1.12347390822228156181    # output: v_y

roldan@pollo:~/research/splitting$ bc -l initcond.bc
Resonance (p/q, p=period of Asteroid, q=period of Jupiter)? 8/1
G = 1.47500000000000000000
e = .67534713296200495530
Initial condition at perihelion (in euclidean coords):
x = 1.29861146815198017877
v_y = 1.13582856472000335952
```

Thus from the 2BP we have the following approximation to an initial condition (at the perihelion):

$$(x, y, p_x, p_y) = (1.3025, 0, 0, 1.1234) \qquad \text{for } \Gamma_7 \tag{6}$$

$$(x, y, p_x, p_y) = (1.2986, 0, 0, 1.1358) \qquad \text{for } \Gamma_8. \tag{7}$$

We refine to obtain the true periodic orbits:

```
# Symmetric resonant 7:1 periodic orbit:
roldan@pollo:~/research/splitting/connect78$ portbpsym <portbpsym7.dat
iter =   1 x =  1.3019610882, PX =  1.0037e-05
iter =   2 x =  1.3019618967, PX =  2.1996e-11
iter =   3 x =  1.3019618967, PX =  1.9761e-15
# output: x, period/2
1.301961896721998e+00 2.199257575905967e+01

# Symmetric resonant 8:1 periodic orbit:
roldan@pollo:~/research/splitting/connect78$ portbpsym <portbpsym8.dat
iter =   1 x =  1.2980565203, PX = -4.6678e-06
iter =   2 x =  1.2980568305, PX = -1.9871e-12
iter =   3 x =  1.2980568305, PX =  6.4560e-16
# output: x, period/2
1.298056830506968e+00 2.513409782621527e+01
```

Thus we find symmetric periodic orbits passing through the points $(x, p_x) = (1.30196, 0)$ and $(x, p_x) = (1.29805, 0)$, with the correct periods $T_{7:1} \simeq 14\pi$ and $T_{8:1} \simeq 16\pi$.

After computing the periodic orbits, we compute their hyperbolic invariant manifolds. We compute the derivative of the 2D Poincare map evaluated at the fixed point:

```
# Resonant 7:1 periodic orbit:
roldan@pollo:~/research/splitting/connect78$ dprtbp_2d <dprtbp_2d_7.dat
 1.2658907713e+00  1.6232238702e-04
 3.7116225998e+03  1.2658907674e+00

# Resonant 8:1 periodic orbit:
roldan@pollo:~/research/splitting/connect78$ dprtbp_2d <dprtbp_2d_8.dat
```

```
 1.3342774290e+00  1.2561294528e-04
 6.2119095309e+03  1.3342774247e+00
```

Compute eigenvalues/vectors:

```
# Resonant 7:1 periodic orbit:
octave:1> M=[
> 1.2658907713e+00,  1.6232238702e-04;
> 3.7116225998e+03,  1.2658907674e+00 ];
octave:2> [evects, evals] = eig(M);
octave:3> format long
octave:4> diag(evals)
ans =

  2.042086260265088
  0.489695278434912

octave:5> evects
evects =

    2.09125646539071e-04   -2.09125645488317e-04
    9.99999978133232e-01    9.99999978133232e-01

octave:6> # Test symplecticity:
octave:6> 2.042086260265088*0.489695278434912
ans = 0.999999999808620

# Resonant 8:1 periodic orbit:
octave:7> M=[
>  1.3342774290e+00,  1.2561294528e-04;
>  6.2119095309e+03,  1.3342774247e+00];
octave:8> [evects, evals] = eig(M);
octave:9> diag(evals)
ans =

  2.217621217222272
  0.450933636477728

octave:10> evects
evects =

    1.42201649782093e-04   -1.42201649089874e-04
    9.99999989889345e-01    9.99999989889345e-01

octave:11> # Test symplecticity:
octave:11> 2.217621217222272*0.450933636477728
ans = 0.999999999812205
```

Thus Γ_8 is slightly more hyperbolic than Γ_7.

Finally, compute the invariant manifolds:

```
roldan@pollo:~/research/splitting/connect78$ invmfld <stmfld7.dat
>stmfld7.res
Estimated error of manifold: 4.888741e-09

roldan@pollo:~/research/splitting/connect78$ invmfld <unstmfld8.dat
```

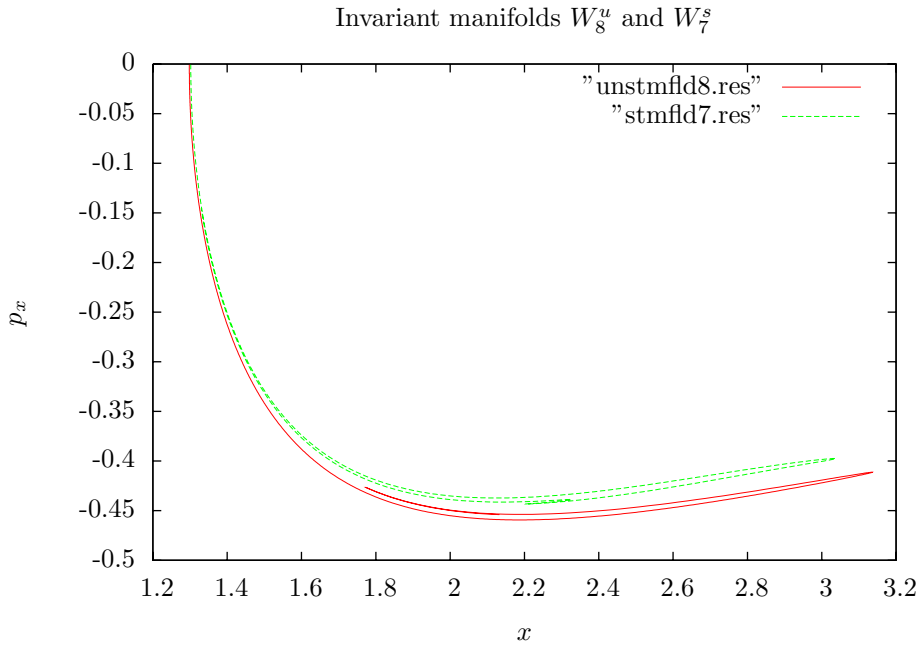

FIGURE 26

```
>unstmfld8.res
Estimated error of manifold: 7.755391e-09
```

The manifolds are plotted in figures 26 and 27.

Unfortunately, the pieces of manifolds that we have computed so far do not intersect.

15. CONNECTING RESONANT 22:3 AND 23:3 ORBITS

Let's try other resonances in between the 7:1 and the 8:1. We start with e.g. the 15:2. The associated periodic orbit should be closer, and the manifolds are more likely to intersect.

```
# 15:2 resonant periodic orbit
roldan@pollo:~/research/splitting$ bc -l initcond.bc
Resonance (p/q, p=period of Asteroid, q=period of Jupiter)? 7.5
G = 1.46950441196103788015
e = .66060909407979723042
Initial condition at perihelion (in euclidean coords):
x = 1.30039226237622183524
v_y = 1.13004702848338658691

roldan@pollo:~/research/splitting/connect78$ portbpsym <portbpsym152.dat
iter =   1 x =  1.2899133592, PX =  4.3411e-02
iter =   2 x =  1.2885270066, PX =  9.1810e-04
iter =   3 x =  1.2884965118, PX =  2.8660e-07
iter =   4 x =  1.2884965023, PX =  2.5271e-14
# output: x, half_period
1.288496502319741e+00 4.398345642247595e+01
```

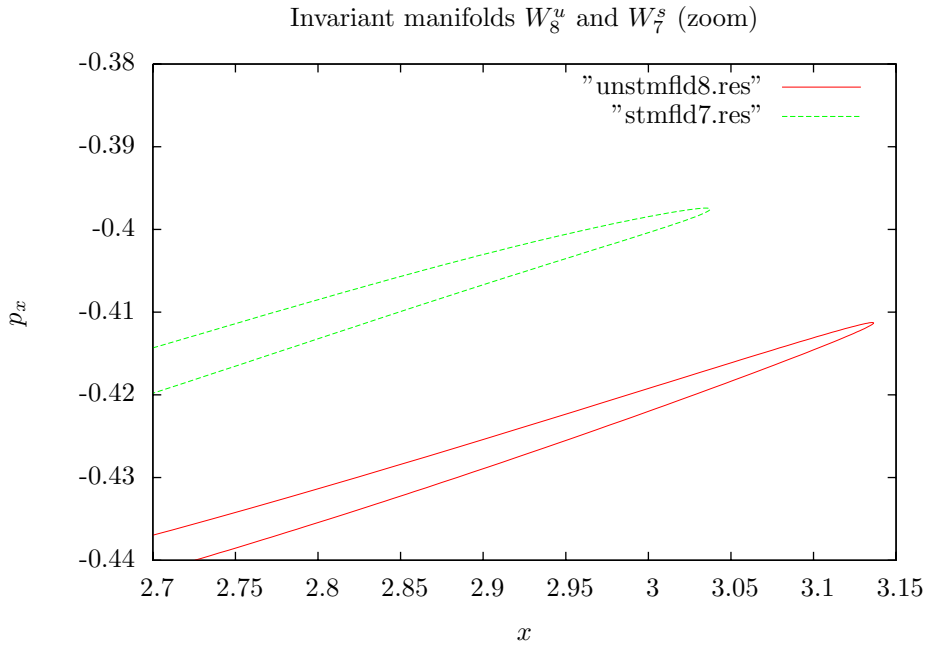

FIGURE 27

The problem when trying to compute the 15:2 periodic orbit is that the Newton method converges to the wrong periodic orbit. In particular, note that the half period obtained is 43.983, whereas we are looking for half-period $15\pi = 47.123$.

Let's try now the 22:3 and 23:3 periodic orbits. Initial conditions:

```
# 22:3 resonant periodic orbit
Resonance (p/q, p=period of Asteroid, q=period of Jupiter)? 7.3333333333333333333
G = 1.46\ 753462083519417937
e = .65530892644628352172
Initial condition at perihelion (in euclidean coords):
x = 1.30106098562127554633
v_y = 1.12795221519491267400

# 23:3 resonant periodic orbit
Resonance (p/q, p=period of Asteroid, q=period of Jupiter)? 7.66666666666666666666
G = 1.47\ 140257174563659372
e = .66570757089910450874
Initial condition at perihelion (in euclidean coords):
x = 1.29976327535754083319
v_y = 1.13205427453001467915
```

Refine periodic orbits:

```
# 22:3 resonant periodic orbit
roldan@pollo:~/research/splitting/connect78$ portbpsym <portbpsym223.dat
iter =   1 x =  1.3005396932, PX =  4.2305e-03
iter =   2 x =  1.3002987781, PX =  2.0885e-03
iter =   3 x =  1.3013461566, PX =  3.0274e-02
...
```

```
iter =  10 x =  1.2999256706, PX = -3.0029e-09
main: unable to find periodic orbit up to desired accuracy
1.299925670618873e+00 6.914163447968416e+01

# 23:3 resonant periodic orbit
roldan@pollo:~/research/splitting/connect78$ portbpsym <portbpsym233.dat
iter =   1 x =  1.2997530192, PX = -1.8363e-04
iter =   2 x =  1.2997521734, PX = -1.2262e-06
iter =   3 x =  1.2997521677, PX = -5.6028e-11
iter =   4 x =  1.2997521677, PX = -3.4963e-15
1.299752167708986e+00 7.228528203030096e+01
```

This time, the half-periods are correct. We are not able to obtain the 22:3 with a lot of accuracy, only 10^{-9}, but we will use this orbit nonetheless.

Derivative (2D):

```
roldan@pollo:~/research/splitting/connect78$ dprtbp_2d <dprtbp_2d_223.dat
 1.1410166321e+02  2.8682531086e-02
 5.0220818044e+05  1.2625233809e+02

roldan@pollo:~/research/splitting/connect78$ dprtbp_2d <dprtbp_2d_233.dat
 2.7683523791e+02  6.9331197838e-02
 1.1053772888e+06  2.7683661967e+02
```

Eigenvalues/vectors:

```
# Resonant 22:3 periodic orbit:
octave:1> M=[
> 1.1410166321e+02,  2.8682531086e-02;
> 5.0220818044e+05,  1.2625233809e+02];
octave:2> [evects, evals] = eig(M);
octave:3> format long
octave:4> diag(evals)
ans =

   4.16065641549206e-03
   2.40349840643585e+02

octave:5> evects
evects =

   -2.51386134996544e-04   -2.27191638951380e-04
    9.99999968402505e-01   -9.99999974191979e-01

octave:6> # Test symplecticity:
octave:6> 4.16065641549206e-03*2.40349840643585e+02
ans = 1.00001310643623

# Resonant 23:3 periodic orbit:
octave:7> M=[2.7683523791e+02,  6.9331197838e-02;
> 1.1053772888e+06,  2.7683661967e+02];
octave:8> [evects, evals] = eig(M);
octave:9> diag(evals)
ans =

   1.80608128806509e-03
```

```
   5.53670051498712e+02

octave:10> evects
evects =

   -2.50443724248595e-04   -2.50442474213983e-04
    9.99999968638970e-01   -9.99999968639283e-01

octave:11> # Test symplecticity:
octave:11> 1.80608128806509e-03*5.53670051498712e+02
ans = 0.999973119773858
```